LAWRENCE
LIVERMORE
NATIONAL
LABORATORY

LLNL-TR-725339

Earthquake Ground Motion Simulation Using Irikura Recipe

A. Pitarka

February 28, 2017

Disclaimer

This document was prepared as an account of work sponsored by an agency of the United States government. Neither the United States government nor Lawrence Livermore National Security, LLC, nor any of their employees makes any warranty, expressed or implied, or assumes any legal liability or responsibility for the accuracy, completeness, or usefulness of any information, apparatus, product, or process disclosed, or represents that its use would not infringe privately owned rights. Reference herein to any specific commercial product, process, or service by trade name, trademark, manufacturer, or otherwise does not necessarily constitute or imply its endorsement, recommendation, or favoring by the United States government or Lawrence Livermore National Security, LLC. The views and opinions of authors expressed herein do not necessarily state or reflect those of the United States government or Lawrence Livermore National Security, LLC, and shall not be used for advertising or product endorsement purposes.

This work performed under the auspices of the U.S. Department of Energy by Lawrence Livermore National Laboratory under Contract DE-AC52-07NA27344.

Earthquake Ground Motion Simulation Using Irikura Recipe

Work for Georesearch Institute, Osaka, Japan

Report Submitted on February 25, 2017

Arben Pitarka

Lawrence Livermore National Laboratory

Task1: Performance of Irikura's Recipe Rupture Model Generator in Earthquake Ground Motion Simulations as Implemented in the Graves and Pitarka Hybrid Approach.

We analyzed the performance of the Irikura and Miyake (2011) (IM2011) asperity-based kinematic rupture model generator, as implemented in the hybrid broadband ground-motion simulation methodology of Graves and Pitarka (2010), for simulating ground motion from crustal earthquakes of intermediate size. The primary objective of our study is to investigate the transportability of IM2011 into the framework used by the Southern California Earthquake Center broadband simulation platform. In our analysis, we performed broadband (0 - 20Hz) ground motion simulations for a suite of M6.7 crustal scenario earthquakes in a hard rock seismic velocity structure using rupture models produced with both IM2011 and the rupture generation method of Graves and Pitarka (2016) (GP2016). The level of simulated ground motions for the two approaches compare favorably with median estimates obtained from the 2014 Next Generation Attenuation-West2 Project (NGA-West2) ground-motion prediction equations (GMPEs) over the frequency band 0.1–10 Hz and for distances out to 22 km from the fault. We also found that, compared to GP2016, IM2011 generates ground motion with larger variability, particularly at near-fault distances (<12km) and at long periods (>1s). For this specific scenario, the largest systematic difference in ground motion level for the two approaches occurs in the period band 1 – 3 sec where the IM2011 motions are about 20 – 30% lower than those for GP2016. We found that increasing the rupture speed by 20% on the asperities in IM2011 produced ground motions in the 1 – 3 second bandwidth that are in much closer agreement with the GMPE medians and similar to those obtained with GP2016. The potential implications of this modification for other rupture mechanisms and magnitudes are not yet fully understood, and this topic is the subject of ongoing study.

This work was performed under the auspices of the U.S. Department of Energy by Lawrence Livermore National Laboratory under Contract DE-AC52-07NA27344.
Release Number:LLNL-TR-725339.

Introduction

The broadband ground motion simulation method of Graves and Pitarka (2010, 2016) and that of Irikura and Miyake (2011, IM2011 hereafter, also known as Irikura's recipe) use similar time-domain summation schemes based on kinematic rupture descriptions. Both methods compute ground motion acceleration time series using rupture kinematics for modeling the source, and Green's functions for modeling wave propagation. Earlier versions of the Irikura and Miyake method employed empirical Green's functions. However, the scarcity of empirical Green's functions with desired magnitude, distance, focal mechanism and source function motivated several modifications of the method including the use of synthetic Green's functions for periods longer than 1 second (e.g., Kamae et al. 1998, Pitarka et al., 2002). At shorter periods, the simulation still relies on the use of empirical Green's functions, and the full broadband response is obtained using a hybrid approach. These modifications as well as the adoption of improved empirical relations of rupture parameters extended the method's applicability to earthquakes of various types and with complex rupture. (e.g. Miyake et al., 2003; Pitarka et al. 2000; Morikawa et. al., 2011; Pitarka et al.,2012; Kurahashi and Irikura,2013; Pulido et al., 2015).

In this article we analyze the performance of the IM2011 asperity-based earthquake rupture model generator implemented in the hybrid broadband ground-motion simulation methodology of Graves and Pitarka (2010). The term hybrid simulation procedure refers to a general approach where the long period motions (typically > 1 s) are computed using a more deterministic approach and the shorter period motions (typically < 1 s) are computed using a more stochastic approach. The full broadband response is then obtained by filtering and summing the individual responses. The IM2011 hybrid method has been validated against several earthquakes in a broad magnitude range (e.g. Iwaki et al., 2016), and is widely used to model and simulate ground motion from earthquakes in Japan. An essential part of the method is its kinematic rupture generation technique, which is based on a deterministic rupture asperity modeling approach. The source model simplicity and efficiency of the IM2011 at reproducing ground motion from earthquakes recorded in Japan makes it attractive to developers and users of the Southern California Earthquake Center Broadband Platform (SCEC BBP) (Maechling et. al, 2015; Graves and Pitarka, 2015; Olsen and Takedatsu, 2015; Schmedes et al., 2010).

The primary objective of our study is to investigate the transportability of the IM2011 rupture generation process to broadband simulation methods used by the SCEC BBP. Here we test it using the Graves and Pitarka (2010) hybrid simulation method. At longer periods (> 1 s), the simulation approach of Graves and Pitarka (2010) is very similar to IM2011; that is, the full kinematic rupture description is convolved with full waveform Green's functions to obtain the ground motion response. However, at shorter periods, the Graves and Pitarka (2010) approach uses a semi-stochastic procedure (following from Boore, 1983) to generate the response, in contrast to the empirical Green's function approach used in IM2011. Therefore, part of our analysis includes formulating the IM2011 rupture such that it can be inserted into the Graves and Pitarka (2010) method at shorter periods. This process is relatively straightforward, but does require some care to insure that all parameters, and in particular the rupture speed, are properly represented.

In order to test the implementation process, we performed broadband (0-20Hz) ground motion simulations for a series of M6.7 scenario oblique-slip earthquakes with rupture models produced with both IM2011 and rupture generation method of Graves and Pitarka (2016, GP2016 hereafter). The kinematic ruptures for both methods are formatted into the Standard Rupture Format (SRF), which is the rupture format used by all the simulations codes on the SCEC BBP. Ground motions from the two rupture model approaches are generated using the same hybrid simulation approach as described in Graves and Pitarka (2010). At long periods (T > 1 s), we compute full waveform Green's functions (GFs) for the prescribed 1D seismic velocity model and these GFs are convolved with the respective kinematic rupture descriptions. At short periods (T < 1 s), the rupture models are resampled onto a 2 km X 2 km grid and the ground motions are computed using the Graves and Pitarka (2010) stochastic formulation. The full broadband response is obtained by summing the individual long- and short period responses using a set of match filters with a crossover set at 1 second (e.g. Hartzell et al., 1999).

In the sections that follow, we first provide an overview of the IM2011 and GP2016 rupture generator procedures. We then describe the scenario ground motion calculations for a hypothetical M6.7 oblique-slip rupture that are used to examine and compare the two rupture generator methodologies. The simulation results are also compared with estimates obtained from four NGA-West2 ground motions prediction equations (GMPEs), which provide a common reference point for analyzing the performance of the different approaches. Based on these comparisons, we also examine a modified version of IM2011 where the rupture speed is increased by 20% across the large-slip asperities, which results in an improved fit to the GMPE levels in the 1 – 3 second period bandwidth. We conclude with a summary of our findings based on this initial set of assessments, along with recommendations to guide further testing and validation of the rupture generator methodologies.

IM2011 and GP2016 Rupture Model Generators

IM2011 is based on the multiple-asperity concept of fault rupture. This concept is an extension of the single-asperity model of Das and Kostrov (1986). IM2011 uses three sets of parameters, named outer, inner and extra fault parameters, to characterize the fault rupture kinematics. The outer parameters characterize the rupture area and magnitude, and the inner parameters define the spatial and temporal characteristics of slip distribution determined from estimated stress drop in the asperities and background areas of the fault. The extra fault parameters are the rupture nucleation location (hypocenter), rupture initiation point in each asperity, and rupture velocity. The outer and inner fault parameters are linked to the total seismic moment following empirical scaling laws. The number of asperities, total asperity area, and asperity slip contrast follows Somerville et al. (1999). These kinematic rupture parameters have been found to be compatible with those obtained from rupture dynamics modeling of planar faults with multiple asperities. (e.g., Dalguer et al.,2004). In contrast to other rupture generation methods, the rupture kinematics in IM2011 are directly linked to static stress drop (e.g., Dan et al., 2001).

In IM2011 the asperities are rupture areas with both higher static stress drop (high slip) and shorter slip duration. This means that most of the strong shaking energy is generated in the asperities areas, which cover only a small portion of the fault area. Since both rupture velocity and slip within each asperity are assumed constant, the resulting strong ground motion level is mainly controlled by the stress drop, and width and amplitude of the initial pulse in the Kostrov-like slip velocity function adopted by IM2011 (Nakamura and Miyatake, 2000). However, the assumption that most of the higher-frequency ground motion originates only in the asperities is debatable. Inversions of recorded strong-motion data often indicate that areas of high slip are not necessarily areas that produce large amounts of high-frequency energy (e.g., Frankel, 2004; Kurahashi and Irikura, 2013). We direct the interested reader to Irikura and Miyake (2011), and Morikawa et al. (2011) for a detailed description of IM2011.

The GP2016 rupture generator uses variable spatial and temporal kinematic rupture parameters that are calibrated using recorded ground motion and observed rupture kinematics. The rupture process, which is randomly heterogeneous at different scale lengths, controls coherent and incoherent interferences of waves generated at the source. The random perturbations to the rupture kinematics follow empirical rules developed through modeling of past earthquakes..

The GP2016 rupture generation process begins with the specification of a random slip field that is filtered to have a roughly wavenumber-squared falloff (e.g., Mai and Beroza, 2002). The slip values are scaled to have a coefficient of variation of 0.85 and to also match the desired seismic moment. Given a prescribed hypocenter, the rupture propagation times across the fault are determined such that the average rupture speed scales at about 80% of the local shear wave velocity. Additionally, the rupture speed is further reduced by a factor of 0.6 for depths of 5 km and less, which is designed to represent the shallow, weak zone in surface-rupturing events (e.g., Marone and Scholz, 1988; Dalguer et al., 2008; Pitarka et al., 2009). A perturbation is then applied to the rupture time at each subfault that is partially correlated with local slip such that the rupture tends to propagate faster in regions of large slip and slows down in regions of low slip. The slip-rate function is a Kostrov-like pulse (Liu et al., 2006) with a total duration (rise time) that is partially correlated with the square root of the local slip. Additionally, the rise time is scaled up by a factor of 2 within the 0–5 km depth range (Kagawa et al., 2004). The average rise time across the fault is constrained to scale in a self-similar manner with the seismic moment (Somerville et al., 1999).

The Graves and Pitarka simulation approach has been validated against a number of past earthquakes, as well as with various GMPEs. We direct the interested reader to Graves and Pitarka (2010) for a detailed description of their hybrid ground motion simulation method and to Graves and Pitarka (2016) for a detailed description of their latest kinematic rupture model generator.

Ground Motion Simulations Using IM2011 and GP2016 Rupture Model Generators

We investigate the performance of IM2011 in conjunction with the Graves and Pitarka (2010) hybrid simulation method by comparing ground motions simulated with IM2011 and

GP2016 rupture models for a hypothetical earthquake. The earthquake we consider is a M6.7 oblique-slip event on a steeply dipping fault. We compute broadband (0 – 20 Hz) ground motions at 39 stations surrounding the fault, and extending to a closest fault distance of about 22 km. The velocity structure is a simple 1D model with hard-rock site condition. The fault mechanism and earthquake rupture parameters are summarized in Table 1 and the velocity model is listed in Table 2. Figure 1 shows the surface projection of the fault and the station locations. The fault rupture is bilateral and the fault spans from 3 to 19km depth.

Rupture Models

Using the two rupture generators we computed a suite of 10 randomized realizations for the M6.7 scenario earthquake. For IM2011, the difference between various realizations is simply the locations of the large and small asperities within the fault plane. For GP2016, each realization results in a different distribution of slip, rupture speed, rise time, and rake. For the sake of generality, in the analysis shown here, no attempt was made to generate GP2016 models that have similar slip distributions to the IM2011 models. Figure 2 illustrates two representative kinematic rupture models generated with IM2011 and GP2016, named IM and GP, respectively. As dictated by the scaling rules in the recipe, the IM rupture has two asperities, one with bigger area and large slip and the other with smaller area and slip (although still above the background slip value). The rupture speed for the IM model is set at a constant value of 2.52 km/s, which is prescribed by the recipe as 72% of the assumed shear wave velocity of 3.5 km/s, and the rake is constant across the entire fault with a value of 25 degrees. For the GP rupture, the slip, rupture speed and rise time distribution are much more heterogeneous compared to the IM rupture. This larger degree of heterogeneity results from the use of randomized spatial fields to generate these parameters in the GP approach. Additionally, the GP method provides partial correlation between rise time and the square root of local slip, and between rupture speed and local slip. This results in a tendency for the rise time to lengthen and the rupture speed to increase as the slip increases. Since the randomized spatial fields are generated to match a roughly wavenumber squared fall-off, there is sufficient spatial heterogeneity at relatively short length scales. Also apparent in the GP rupture is the systematic reduction of rupture speed and lengthening of rise time along both the top and bottom portions of the rupture. For this buried and dipping fault, this scaling is most prevalent in the upper 4 km of the fault plane, although it is also seen below about 15 km down-dip distance.

Figure 3 shows time series of slip velocity as prescribed by the two rupture models at selected locations on the fault. For IM (Figure 3, left panel), one location is inside the large asperity and the other in the background slip area. The IM procedure requires the total duration (rise time) of the slip velocity function to scale inversely with the local slip. Thus, the rise time for the background area is about twice as long as that for the large asperity, which results in a relatively low peak amplitude and very long tail on the background slip-velocity function. Since the radiated strong motion energy is generally correlated with the peak slip velocity, the scaling prescribed by the IM model means most of the strong motion radiation will come from the asperities, with the background areas mainly providing relatively longer period radiation. As noted above, the GP rupture has a more complex and heterogeneous distribution of rupture parameters, and this is also reflected in the scaling of

the slip velocity functions. For GP (Figure 3, right panel) the functions come from locations that sample both large and small slip, as well as different depths on the fault. Locations 1 and 3 both have slip values of about 200 cm, although the rise time for the slip-velocity function at location 3 is about twice that for location 1. This results from the depth scaling of rise time that is prescribed in the GP approach. Location 2 has roughly the average fault slip (83 cm), but since GP tends to scale rise time with slip, this location has a relatively short rise time, and the peak slip velocity at this site is similar to that at location 3. This highlights some key features of the GP approach whereby large shallow fault slip does not necessarily translate into large strong motion radiation. Additionally, it means that strong radiation of shorter period motion does not necessarily coincide with regions of large slip.

Both set of rupture models were inserted into the Graves and Pitraka (2010) hybrid simulation process as implemented on the SCEC BBP. The low-frequency part of ground motion (0 -1Hz) was calculated using synthetic Green's functions computed with the FK method of Zhu and Rivera (2002). Table 2 describes the flat-layered velocity model used in the simulations. The sub-fault dimensions used in the simulations of the low frequency part of ground motion were 0.1 x 0.1km, and used the full kinematic rupture descriptions as described earlier.

The high frequency simulation approach of Graves and Pitarka (2010) uses a semi-stochastic representation that requires some modification of the full kinematic rupture description. The primary modification is the replacement of the deterministic slip-velocity function with a windowed time series of band-limited white Gaussian noise. This time series is filtered to a target omega-squared spectrum and scaled to match the target moment release on the subfault. A basic premise of this approach is that it is designed to utilize the random phasing of the radiated subfault waveform to represent the poorly constrained and/or unknown details of the rupture process. For this reason, Graves and Pitarka (2010) recommend limiting the subfault size used for the high-frequency calculation to have a minimum characteristic dimension no smaller than about 1-2 km. More details about this can be found in Graves and Pitarka (2010 and 2015). In the scenario simulations considered here, we resample the full kinematic rupture description to a grid of 2km by 2km for insertion in the high-frequency portion of the calculations. Another important input parameter for the high-frequency simulations is the average rupture speed, which is related to the subfault corner frequency in the Graves and Pitarka (2010) approach. For IM, this is set to 72% of the local Vs, and for GP it is set at 77.5% of the local Vs. An additional 60% reduction of rupture speed along the shallow and deep portions of the fault as dictated by Graves and Pitarka (2010, 2015) was applied to both the IM and GP high-frequency rupture simulations.

The matching frequency f_m used to combine the high- and low-frequency portions of the simulated ground motion was set at 1Hz. In many studies the transition between the deterministic and stochastic characteristics of ground motion is made at 1Hz, partly due to computational limitations in wave propagation modeling, and limited reliability of seismic velocity and rupture models. However analysis of observed ground motion has shown that the transition between coherent and incoherent rupture and wave propagation processes generally occurs around 1 Hz (e.g., Liu and Helmberger, 1985; Graves and Pitarka, 2016),

although there may be some variation with magnitude (Frankel, 2009). Therefore fixing f_m at 1Hz is rather arbitrary and subject to further research.

Simulation Results

Figures 4a and 4b compare time series of ground motion acceleration and velocity, respectively, computed with the IM and GP rupture models shown in Figure 3 at 16 selected stations. Despite the noted differences in the rupture models, the ground motions produced with these two rupture models are quite similar. In general, the amplitude of the IM acceleration time histories is slightly larger at all distances. In contrast, the velocity time histories are much more similar. This can be explained by the difference in small-scale rupture complexities between the two models. The GP model, which is more heterogeneous than the IM model, creates more deconstructive waveform interference in both time and space. Later we will show that for the same reason GP produces less intra-event variability in near-fault ground motion. IM produces slightly stronger rupture directivity effects near the asperity area, which results from strong constructive interference due to the smooth rupture at constant rupture speed. This effect is manifested by increased amplitude of the fault normal, east-west (EW), component of ground motion velocity at near-fault locations, such as stations 8, 10, 18, 20 and 22.

From the simulated waveforms for each realization, we compute the RotD50 pseudo spectral acceleration (Boore et al., 2006) at each site. These values are compared with estimates from four NGA-West2 GMPEs (Abrahamson et al., 2014; Boore et al., 2014; Campbell and Bozorgnia, 2014; Chiou and Youngs, 2014) for various oscillator periods in Figures 5a (for GP) and 5b (for IM). In general, the simulated values for both IM and GP lie near the range of the median values of the GMPEs across all periods and distances. It can also be seen in these plots that the variability of the IM responses is greater than that for GP, particularly at the longer periods. We will discuss this further in a later section.

In order to obtain a more quantitative assessment of the comparison between the simulations and GMPEs, we have used the response spectral acceleration goodness-of-fit (GOF) approach described by Goulet et al., 2015. This is done by first computing the residual between the simulated value and the estimated median value from each of the four GMPEs at each site. This is done for all 10 realizations for each of GP and IM. Then for each oscillator period, we compute the median and standard error for all of the residuals (39 sites and 10 realizations compared with four GMPEs for each rupture model generator). The GOF results are shown in Figure 6. For periods shorter than 1 sec, both methods produce similar results, with similar trend down to 0.1 sec. The bias values are centered around zero, with a maximum deviation of about 25%. At longer periods (> 1 sec), the GP results are near zero bias all the way out to 10 sec, whereas the IM results show a systematic under-prediction of the GMPE levels of about 20-30% in the period range 1 – 3 sec.

Given that we are considering a hypothetical earthquake rupture embedded in a very simple 1D velocity structure, we cannot say what the "correct" ground motion response should be. Nonetheless, the systematic difference seen between the GP and IM responses in the 1 – 3 sec period range is intriguing, and warrants further investigation.

Modified IM Approach (IM-fastRS)

One of the main differences in the IM and GP rupture generator approaches involves the specification of the temporal characteristics of the rupture, i.e., the rupture speed and rise time. In IM, the rupture speed is constant across the entire fault, and the rise time does not vary within the large slip asperity regions. The GP ruptures on the other hand incorporate significant variability in the specification of these parameters, as well as partially correlating these with the spatially heterogeneous slip values. Based on these features, we created a modified version of the IM approach such that the rupture speed is increased on the asperity areas by 20%. Due to the coupling of rupture speed and slip velocity function in the IM method, the increase in rupture speed also resulted in a 16% decrease in rise time, and a 9% increase in peak slip velocity in the asperities. Figure 7 plots one realization of the modified IM approach, which we refer to as IM-fastRS.

We generated 10 realizations of the M6.7 scenario using the IM-fastRS approach and ran simulations with these in the exact same manner as was done for IM and GP. We then computed RotD50 values and generated GOF comparisons using the NGA-West2 GMPEs. The GOF for the IM-fastRS rupture simulations is shown in Figure 8. Compared to the GOF for IM (Figure 6, right panel), the IM-fastRS result shows slightly stronger motions (downward shift of the bias level) for periods less than about 1 sec, and a much larger downward shift for periods great than 1 sec. The slight increase in shorter period ground motion levels is not unexpected since the Graves and Pitarka (2010) high frequency simulation approach uses the rupture speed to scale the subfault corner frequency, which in turn controls the level of high-frequency motions. Thus, the increase in average rupture speed translates directly into an increase in high-frequency ground motion levels. Likewise, the increase in longer period ground motion levels is not unexpected, although the magnitude of the ground motion increase in the 1 – 3 sec bandwidth (about 30%) is significantly larger than the 20% change in the rupture speed. We suspect that there is a combination of factors, which are contributing to this ground motion increase. In particular, the increase in peak slip velocity coupled with the increased rupture speed across the large slip asperity time compresses the longer period ground motion radiation into a shorter duration pulse. This can strongly increase the ground motion levels, especially for near fault sites such as those considered in our simulation experiment. A test with increased rupture speed by only 10% produced similar effects but the impact on ground motion amplitude was weak.

In order to examine the distance dependence of these features in more detail, we have separated the residuals into different distance bins (Table 3). Figure 9 plots the residuals in these distance bins for periods of 0.1 to 10 sec for each rupture model. Also shown in these plots is the range of the individual GMPE medians for each period. While a value of zero on these plots represents the average of the median values from the four GMPEs, the spread of the GMPEs varies greatly as a function of period, and in particular, it shows a noticeable increase with increasing period. This degree of variability suggests caution when comparing the simulations with the individual GMPE values.

There are several trends readily apparent from the plots in Figure 9. First there are actually very few places where the median residual lies outside of the maximum-minimum spread of the GMPE medians. This is encouraging because it indicates that all of the rupture generators are producing results that are generally in agreement with the empirical models. Secondly, there are very similar trends that are seen across all models for periods less than 1 second, for example, under-predication at very short periods and slight over prediction around 0.5 sec. Since this is present for all three models, it shows that the high-frequency approach in Graves and Pitarka (2010) tends to smooth out the differences in the different rupture approaches, and the resulting variability is embedded within the stochastic phasing of the method. Thirdly, the variability of the IM and IM-fastRS results is larger than GP, particularly for periods above 1 sec. This is likely due to the large discrete asperities in IM and IM-fastRS compared to the more heterogeneous slip distribution in GP. Thus, asperity proximity, as opposed to simply fault distance, has a much stronger impact on ground motion levels in IM than in GP.

In order to better understand and quantify the ground motion variability produced by the different rupture model generators, we computed the standard deviation of simulated ground motion (sigma) and analyzed its variability as a function of period and distance. Again, we grouped the stations into different distance bins so that we could get enough observations to perform the statistical analysis of sigma. The distance bins and number of stations in each bin are shown in Table 3.

For each distance bin and period we computed the standard deviation (sigma) of simulated spectral acceleration. We then calculated the average sigma over ten rupture realizations for the IM, IM-FastRS and GP models. Similarly, we calculated the median ground motion for each model, and its standard deviation as a function of distance bin and period. The standard deviation of the median is a way to measure how much the median value changes from realization to realization within each of the three rupture generators. If each rupture realization produces the same median level of ground motion then the standard deviation of median would be zero. This means no inter-event variability. If the median level of ground motion changes dramatically from realization to realization, then the sigma of the median would be very high. This would indicate large inter-event variability. The variability of the median maps into the total variability across all simulations, represented by the average sigma. We recognize the set of 10 realizations we have considered for each rupture generator approach is a very limited sample. Furthermore, the current set of realizations only considers variations in slip distribution, which neglects other important sources of event-to-event variability such as changes in hypocenter and fault rupture area (static stress drop). These additional factors would likely have a significant contribution to the simulated inter-event variability. Thus, we regard the current estimate of inter-event sigma as a lower-bound value.

Figure 10 shows sigma (orange lines), average sigma (red lines) and sigma of median (blue line) for IM, IM-FastRS and GP rupture generators. Using the statistical analysis shown in this figure we drew several conclusions about ground motion variability simulated with IM, IM-fastRS and GP. First, the level of intra-event sigma is much larger than inter-event sigma across all distances and periods, and for all three rupture model generators. However, we

must use caution when comparing absolute levels of intra- and inter-event for this limited set of simulations due to the under-sampling of possible event-to-event variability mentioned above. Nonetheless, these current results suggest that variations in slip distribution contribute only a modest amount to the inter-event sigma, with the level being somewhat stronger for IM than for GP. Second, regardless of modification for rupture speed, IM produces more variability than GP across all periods, especially at the longer periods (>1 s) and closer distances (< 12km). The larger variability for IM and IM-fastRS results from their smoother rupture process and simple and well-defined asperity areas. At long periods and short distances these distinct source characteristics generate stronger local directivity effects and consequently stronger ground motion variability depending on the relative location of the station to asperities. The strength of this effect would likely be even greater had we considered different hypocenter locations in our analysis. The long-period intra-event variability for IM is strongest at near-fault distances, and then is substantially reduced beyond 12km. At those distances the intra-event ground motion variability for IM approaches the level found for GP. Third, although to a lesser extent, the larger variability for IM compared to that for GP at near-fault distances is also present at short periods (< 1s). Part of the reason for this is that slip resampling on a coarser 2km x 2km grid, required by the high frequency modeling in Graves and Pitarka (2010) method affects the IM and GP models differently. In the case of GP models it tends to reduce the original small-scale spatial complexity of slip. Consequently the source contribution to short-period ground motion variability is reduced. This explains the gradual increase of ground motion variability with period at near-fault distances observed for GP models. In contrast, because of the geometrical simplicity of the asperity area in IM models, slip resampling does not modify the spatial characteristics of the original slip, and therefore it has a smaller impact on simulated ground motion especially at short periods. At those periods sigma for IM models remains roughly constant at all distances.

Conclusions

In this study we investigate the transportability of the IM2011 asperity-based kinematic rupture model generator into the simulation framework used by the Southern California Earthquake Center broadband simulation platform. For this purpose we implemented IM2011 within the hybrid broadband ground-motion simulation methodology of Graves and Pitarka (2010), which is one of the simulation approaches currently installed on the SCEC BBP. The performance of the IM2011 rupture model was investigated by comparing ground motions simulated using this approach with those obtained from the GP2016 rupture generator and NGA-West2 GMPEs for a suite of realizations of a hypothetical M6.7 crustal earthquake embedded in a hard-rock velocity structure. Despite conceptual differences between the two rupture generation approaches the simulations show both models produce ground motions that are similar to those obtained from NGA-West2 GMPES across the period range 0.1 to 10 seconds. The largest difference found for this M6.7 scenario is in the period range 1 – 3 s where the IM ground motion amplitude is somewhat lower (~20-30%) compared with both GP2016 and the GMPE medians. One possible cause for this band-limited discrepancy is related to the assumption of constant rupture speed over the entire fault made in IM2011. In contrast, GP2016 uses spatially heterogeneous slip and by association heterogeneous rupture speed, and these rupture parameters contain

deterministic and stochastic features that are modeled using magnitude and depth dependent empirical relationships. We found that the amplitude of ground motion produced with IM in the 1-3 s period band is sensitive to the rupture speed across the asperities. Increasing the asperity rupture speed by 20%, produces ground motions closer to both the GP results and the GMPE median. Further testing is needed to determine how this modification can be generalized to other rupture geometries and magnitudes, and other velocity structures.

Another important observation made in this study is that the IM model produces larger intra-event ground motion variability than the GP model, particularly for periods greater than 1 s. This is likely due to the discrete asperities in the IM model compared to the more heterogeneous slip distribution in the GP model. Consequently, the asperity proximity, as opposed to simply fault distance, has a much stronger impact on ground motion levels in IM than in GP. We also find that event-to-event variations in slip distribution only contribute a modest amount to the overall level of ground motion variability (sigma). The amount of variability due to this effect is slightly larger for IM than for GP, which again is likely due to the use of large discrete asperities in the IM approach. Furthermore, we recognize that there are other important sources of event-to-event variability that we have not considered in the current study, most notably changes in hypocenter and fault rupture area. Incorporation of this additional variability in the simulations would probably result in a significant increase in the level of inter-event sigma, and this topic is the subject of future work.

References

Abrahamson, N. A., W. J. Silva, and R. Kamai (2014), Summary of the ASK14 Ground Motion Relation for Active Crustal Regions, Earthq. Spectra, 30(3), 1025–1055, doi:10.1193/070913EQS198M.

Boore D. (1983), Stochastic simulation of high frequency ground motions based on seismological models of the radiated spectra. Bull. Seism. Soc. Am. 1983; 73: 1865-1894.

Boore, D. M., Watson-Lamprey, J., and Abrahamson, N. A., (2006). Orientation independent measures of ground motion, Bull. Seism. Soc. Am. 96, 1502-1511.

Boore, D. M., J. P. Stewart, E. Seyhan, and G. M. Atkinson (2014), NGA-West2 Equations for Predicting PGA, PGV, and 5% Damped PSA for Shallow Crustal Earthquakes, Earthq. Spectra, 30(3), 1057–1085, doi:10.1193/070113EQS184M.

Campbell, K. W., and Y. Bozorgnia (2014), NGA-West2 Ground Motion Model for the Average Horizontal Components of PGA , PGV , and 5 % -Damped Linear Acceleration Response Spectra, Earthq. Spectra, 30(3), 1087–1115, doi:10.1193/062913EQS175M.

Chiou, B. S. J., and R. R. Youngs (2014). Update of the Chiou and Youngs NGA Ground Motion Model for Average Horizontal Component of Peak Ground Motion and Response Spectra, , 30(3), 1117–1153, doi:10.1193/072813EQS219M.

Dalguer, L. A., H. Miyake, and K. Irikura (2004), Characterization of dynamic asperity source models for simulating strong ground motions, Proceedings of the 13th World Conference on Earthquake Engineering No. 3286.

Dalguer, L. A., H. Miyake, S. M. Day, and K. Irikura (2008). Surface-rupturing and buried dynamic rupture models calibrated with statistical observations of past earthquakes, Bull. Seismol. Soc. Am. 98, 1147–1161.

Dan, K., M. Watanabe, T. Sato, and T. Ishii (2001), Short- period source spectra inferred from variable-slip rupture models and modeling of earthquake fault for strong motion prediction, J Struct Constr Eng AIJ 545, 51–62.

Das, S., and B. V. Kostrov (1986). Fracture of a single asperity on a finite fault, In Earthquake Source Mechanics. Geophysical Monograph 37, Maurice Ewing Series 6, American Geophysical Union, pp. 91–96.

Frankel, A. (2004). Rupture process of the M 7.9 Denali Fault, Alaska, earth- quake: subevents, directivity, and scaling of high-frequency ground motions, Bull. Seismol. Soc. Am. 94, S234–S255.

Frankel, A. (2009), A constant stress-drop model for producing broadband synthetic seismograms: Comparison with the next generation attenuation relations, Bull. Seismol. Soc. Am., 99(2 A), 664–680, doi:10.1785/0120080079.

Goulet, C. A., N. A. Abrahamson, P. G. Somerville, and K. E. Woodell (2015). The SCEC Broadband Platform validation exercise for pseudo-spectral acceleration: Methodology for code validation in the context of seismic hazard analyses, Seismol. Res. Lett 86, no. 1, doi: 10.1785/0220140101.

Graves, R., and Pitarka, A (2016), Kinematic ground motion simulations on rough faults including effects of 3D Stochastic velocity perturbations. Bull Seismol Soc Am

Graves, R., and Pitarka, A. (2015) Refinements to the Graves and Pitarka (2010) Broadband Ground-Motion Simulation Method Seismological Research Letters, January/February 2015, v. 86, p. 75-80, First published on December 17, 2014, doi:10.1785/0220140101

Graves, R. W. and A. Pitarka (2010). "Broadband Ground-Motion Simulation Using a Hybrid Approach." Bull. Seis. Soc. Am., 100(5A), pp. 2095-2123, doi: 10.1785/0120100057.

Hartzell, S., and T. H. Heaton (1983). Inversion of strong ground motion and teleseismic waveform data for the fault rupture history of the 1979 Imperial Valley, California, earthquake, Bull. Seismol. Soc. Am. 73, 1553–1583.

Irikura, K. and H. Miyake (2001), Prediction of strong ground motions for scenario earthquakes, Journal of Geography 110, 849–875 (in Japanese with English abstract).

Irikura K, H. Miyake, T. Iwata, K. Kamae, and H. Kawabe (2002), Revised recipe for predicting

strong ground motion and its validation, Proceedings of the 11th Japan Earthquake Engineering Symposium, 567–572 (in Japanese with English abstract).

Irikura K, H. Miyake, T. Iwata, K. Kamae, H. Kawabe and Dalguer, L. A. (2004), Recipe for predicting strong ground motion from future large earthquake, Proceedings of the 13th World Conference on Earthquake Engineering No. 1371.

Irikura, K. (2004), Recipe for predicting strong ground motion from future large earthquake, Annuals of Disaster Prevention Research Institute 47A, 25–45 (in Japanese with English abstract).

Irikura, K., and H. Miyake (2011). Recipe for Predicting Strong Ground Motion from Crustal Earthquake Scenarios, Pure Appl. Geophys. 168 (2011), 85–104 . DOI 10.1007/s00024-010-0150-9 .

Iwaki, A., T. Maeda, N. Morikawa, H. Miyake, H. Fujiwara (2016) Validation of the Recipe for Broadband Ground-Motion Simulations of Japanese Crustal Earthquakes, Bull. Seis. Soc. Am., (in press)

Kagawa, T., K. Irikura, and P. Somerville (2004), Differences in ground motion and fault rupture process between the surface and buried rupture earthquakes, Earth Planets Sp., 56(2003), 3–14.

Kamae, K., K. Irikura, and A. Pitarka (1998), A technique for simulating strong ground motion using hybrid Green's function, Bull Seism. Soc. Am. 88, 357–367.

Kurahashi, S., and K. Irikura (2013) Short-Period Source Model of the 2011 M_w 9.0 Off the Pacific Coast of Tohoku Earthquake, Bull. Seism. Soc. Am., 103, 1373-1393, doi:10.1785/0120120157.

Maechling, P. J., F. Silva, S. Callaghan, and T. H. Jordan (2015). SCEC Broadband Platform: System Architecture and Software Implementation, Seismol. Res. Lett., 86, no. 1, doi: 10.1785/0220140125.

Liu, H.-L., and D. V Helmberger (1985), The 23:19 Aftershock of the 15 October 1979 Imperial Valley Earthquake: More Evidence for an Asperity, Bull. Seism. Soc. Am., 75(3), 689–708, doi:10.1017/CBO9781107415324.004.

Liu, P., R. J. Archuleta, and S. H. Hartzell (2006), Prediction of broadband ground-motion time histories: Hybrid low/high-frequency method with correlated random source parameters, Bull. Seismol. Soc. Am., 96(6), 2118–2130, doi:10.1785/ 0120060036.

Mai, P. M., and G. C. Beroza (2002), A spatial random field model to characterize complexity in earthquake slip, J. Geophys. Res., 107(10.1029), 2001, doi:10.1029/2001JB000588.

Marone, C., and C. H. Scholz (1988), The Depth of Seismic Faulting and the Upper Transition from Stable to Unstable Slip Regimes, Geophys. Res. Lett., 15(8), 621–624.

Miyake, H., T. Iwata, and K. Irikura (2003), Source characterization for broadband ground-motion simulation: kinematic heterogeneous source model and strong motion generation area, Bull Seismol Soc Am 93, 2531–2545.

Morikawa, N., S. Senna, Y. Hayakawa, and H. Fujiwara (2011), Shaking maps for scenario earthquakes by applying the upgraded version of the strong ground motion prediction method ''Recipe'', Pure Appl. Geophys. 168 (2011), 645–657, DOI:10.1007/s00024-010-0147-4.

Nakamura, H., and T. Miyatake (2000), An approximate expression of slip velocity time functions for simulation of near-field strong ground motion, Zisin 53, 1–9 (in Japanese with English abstract).

Olsen, K. B., and Takedatsu, R. (2015) The SDSU Broadband Ground-Motion Generation Module BB toolbox Version 1.5 Seismological Research Letters, January/February 2015, v. 86, p. 81-88, First published on December 17, 2014, doi:10.1785/0220140102.

Pitarka, A, L. Dalguer, S. Day, P. Somerville, and K.Dan (2009). Numerical study of ground-motion differences between buried-rupturing and surface-rupturing earthquakes. Bull. Seism. Soc. Am. 99, 1521-1537.

Pitarka A., P. Somerville, Y. Fukushima, T. Uetake, and K. Irikura. (2000). Simulation of near-fault strong ground motion using hybrid Green's functions, Bull. Seism. Soc. Am., 90, 566-586.

Pitarka, A., P. Somerville, Y. Fukushima (2002) Ground-motion attenuation from the 1995 Kobe earthquake based on simulations using the hybrid Green's function method. Bull. Seism. Soc. Am., 92, 1025-1031.

Pitarka, A., S. Matsuzaki, T. Watanabe, N. Collins, R. Graves, and P.Somerville (2012). Rupture Model for a Characterized Intraslab earthquake. Proceedings of the 15th Word Conference of earthquake Engineering, September 24-28, Lisbon, Portugal.

Pulido, N., Z. Aguilar, H. Tavera, M. Chlieh, D. Calderon, T. Sekiguchi, S. Nakai, and F. Yamamzaki (1015). Scenario source models and strong ground motion for future mega-earthquakes: application to Lima, central Peru. Bull. Seism. Soc. Am., 105, 368-386.

Schmedes, J., R. J. Archuleta, and D. Lavallée (2010). "Correlation of earthquake source parameters inferred from dynamic rupture simulations." J. Geophys. Res., 115, B03304, doi:10.1029/2009JB006689.

Somerville, P., K. Irikura, R. Graves, S. Sawada, D. Wald, D., N. Abrahamson, Y. Iwasaki, T. Kagawa, N. Smith, and A. Kowada (1999), Characterizing earthquake slip models for the prediction of strong ground motion, Seism. Res. Lett. 70, 59–80.

Zhu, L., and L. Rivera (2002). A note on the dynamic and static displacements from a point source in multilayered media, Geophys. J. Int. (2002) 148 (3): 619-627. doi: 10.1046/j.1365-246X.2002.01610.x

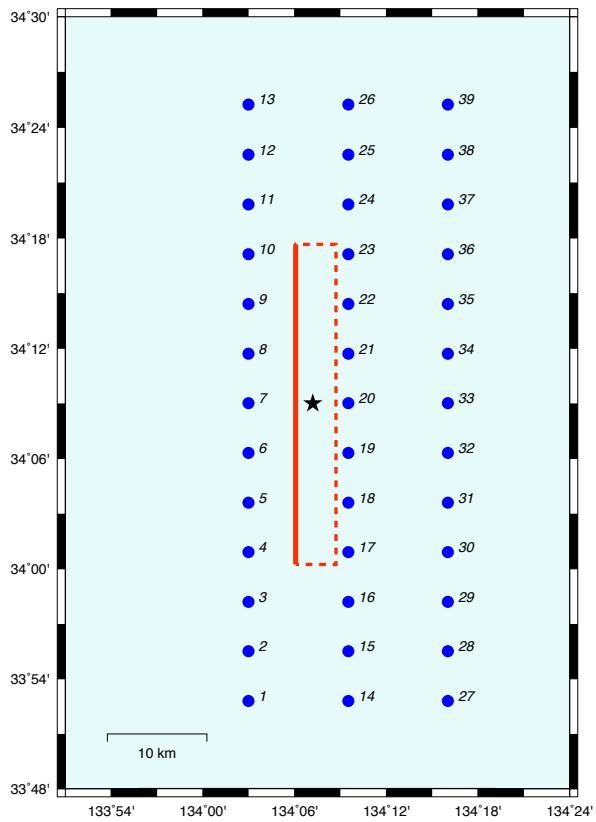

Figure1. Map of station locations (blue circles) and fault trace (red rectangle) for the M6.7 scenario earthquake simulations. Star indicates the rupture initiation location projected on the free surface.

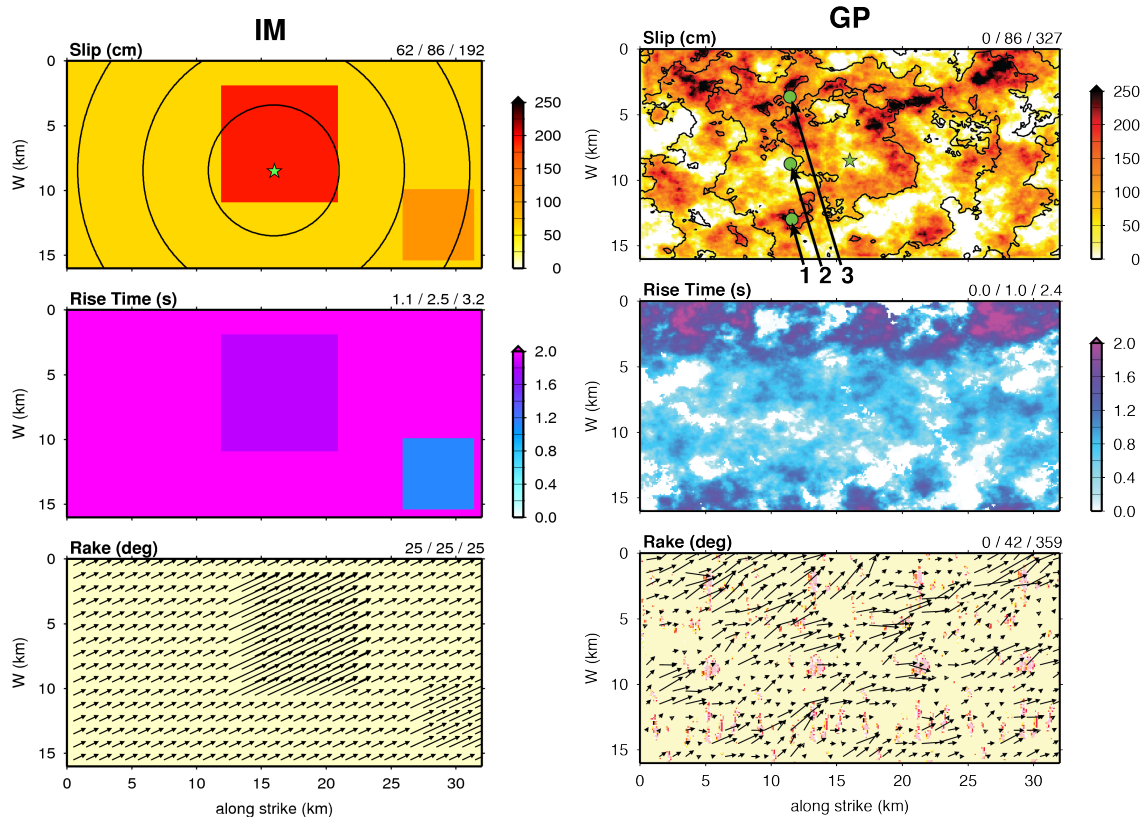

Figure 2. Examples of kinematic rupture models for a scenario M6.7 oblique slip earthquake, created with IM2011 (left panel) and GP2016 (right panel). The triplet of numbers at the upper right of each panel indicate the minimum, average and maximum values of the parameter being displayed.

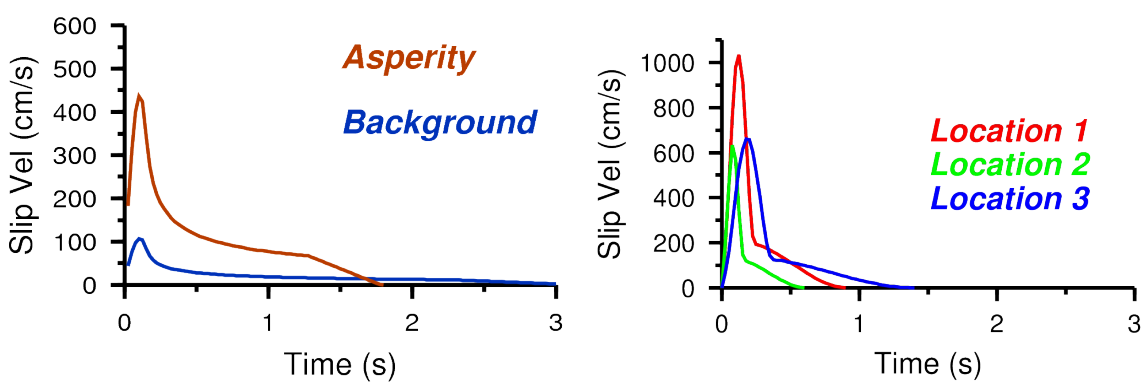

Figure 3. Left panel shows comparison of slip velocity functions in the large slip asperity area (red trace) and background fault area (blue trace) for the IM2011 model. Right panel shows slip velocity functions for 3 locations on the GP2016 rupture (locations indicated in Figure 2). For the GP rupture, locations 1 and 3 both have the same final slip of 200 cm, and location 2 has 83 cm slip.

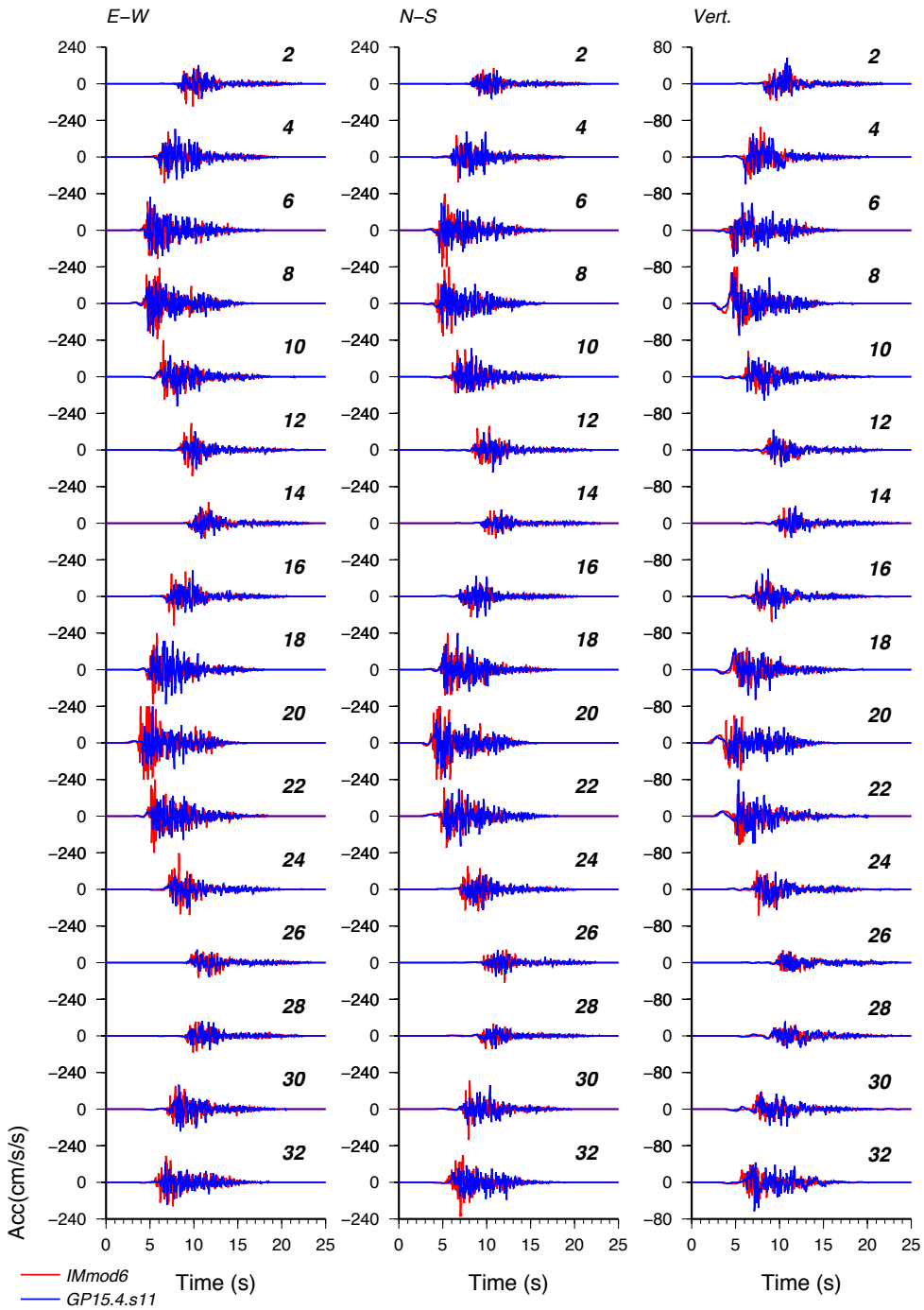

Figure 4a. Comparison of broadband (0 -20Hz) acceleration time series simulated with the GP (blue traces) and IM (red traces) rupture models shown in Figure 3.

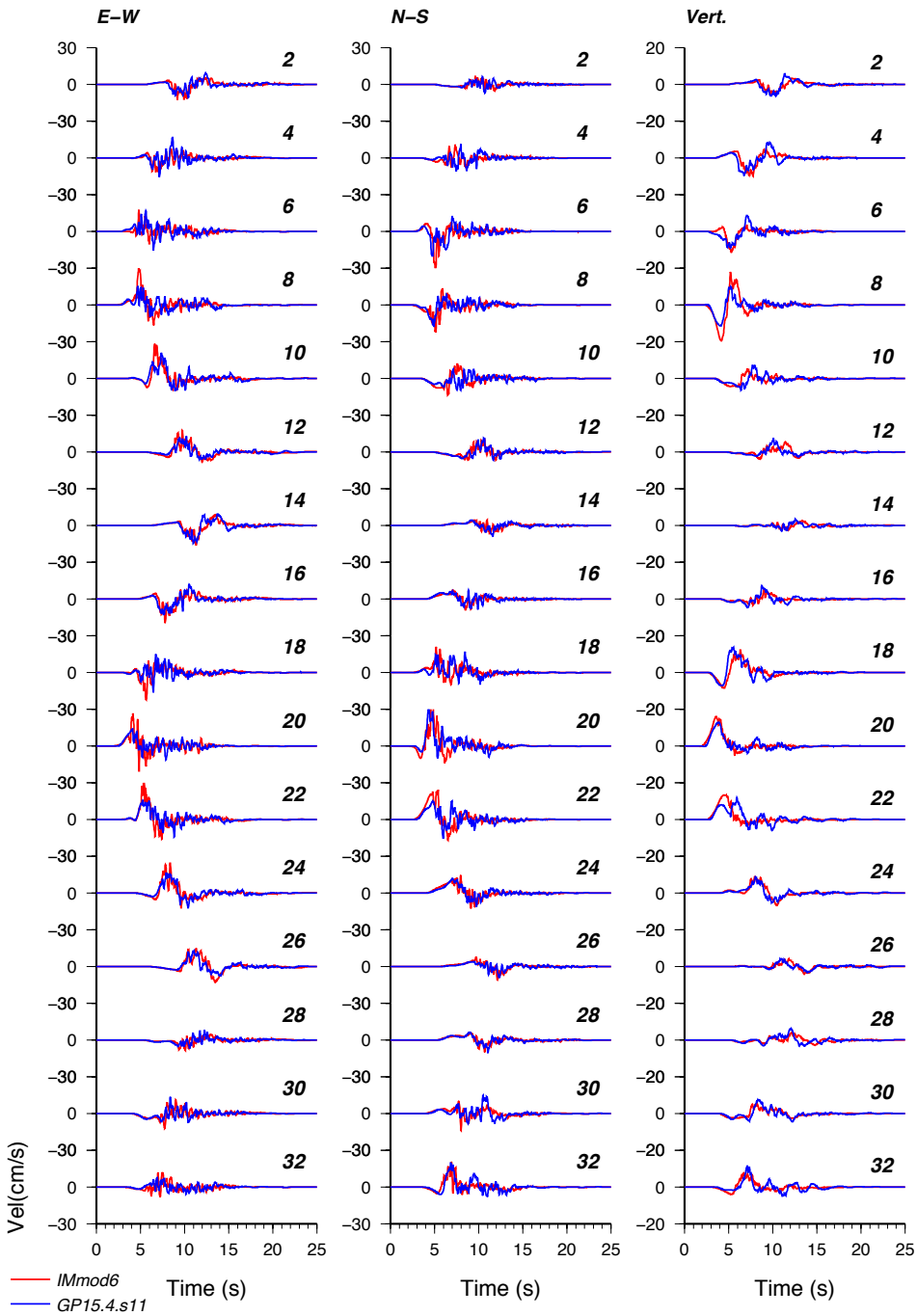

Figure 4b. Comparison of broadband (0 -20Hz) velocity time series simulated with the GP (blue traces) and IM (red traces) rupture models shown in Figure 3.

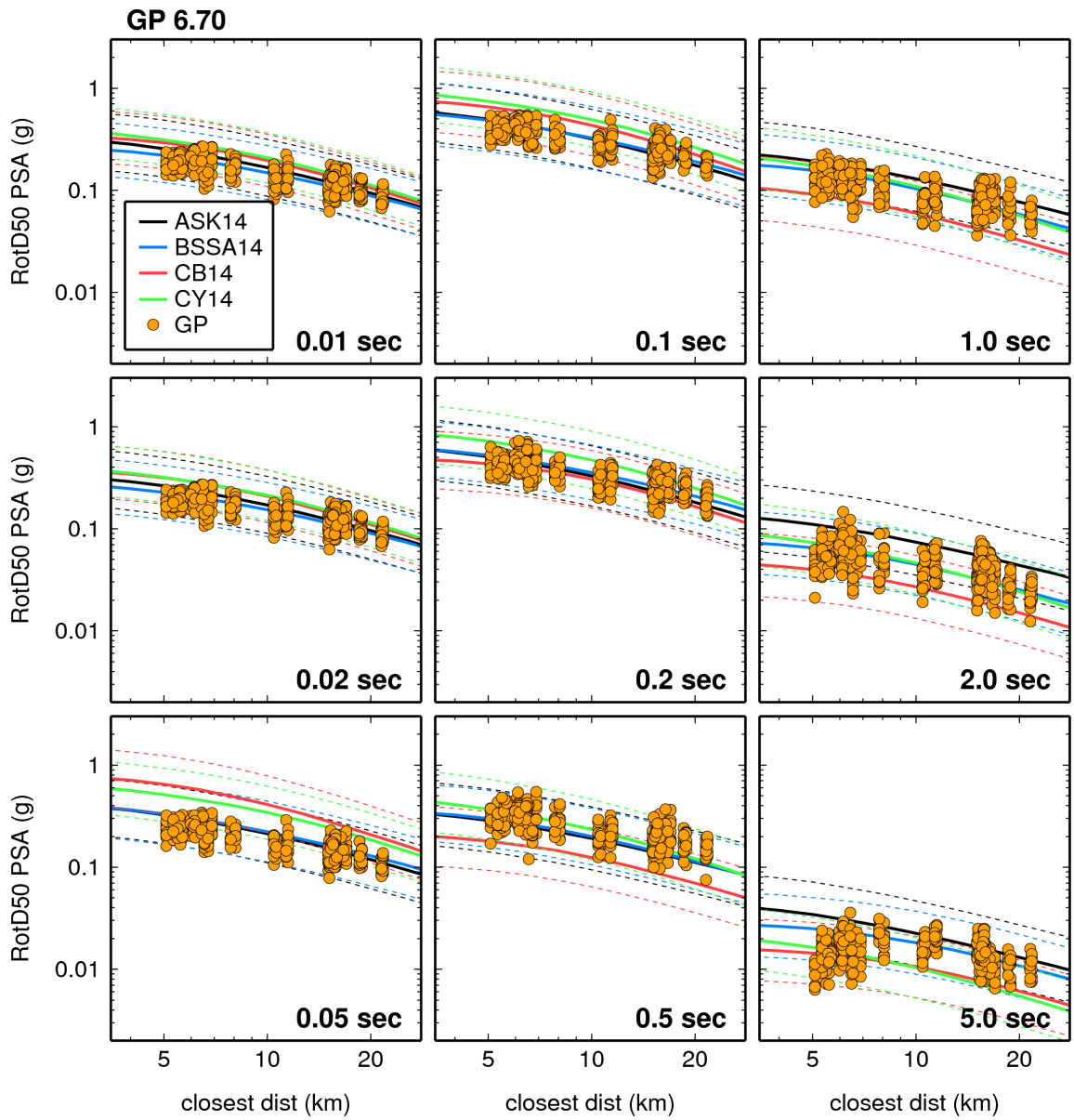

Figure 5a. RotD50 horizontal pseudo-spectral acceleration for 10 random realizations of the scenario M6.7 earthquake computed using the GP method (gold circles) compared with estimates obtained from four NGA-West2 GMPEs. Median values for GMPEs are shown in solid lines with dashed lines indicating +/- one standard deviation (total sigma). GMPEs are ASK14, Abrahamson et al. (2014); BSSA14, Boore et al. (2014); CB14, Campbell and Bozorgnia (2014); CY14, Chiou and Youngs (2014).

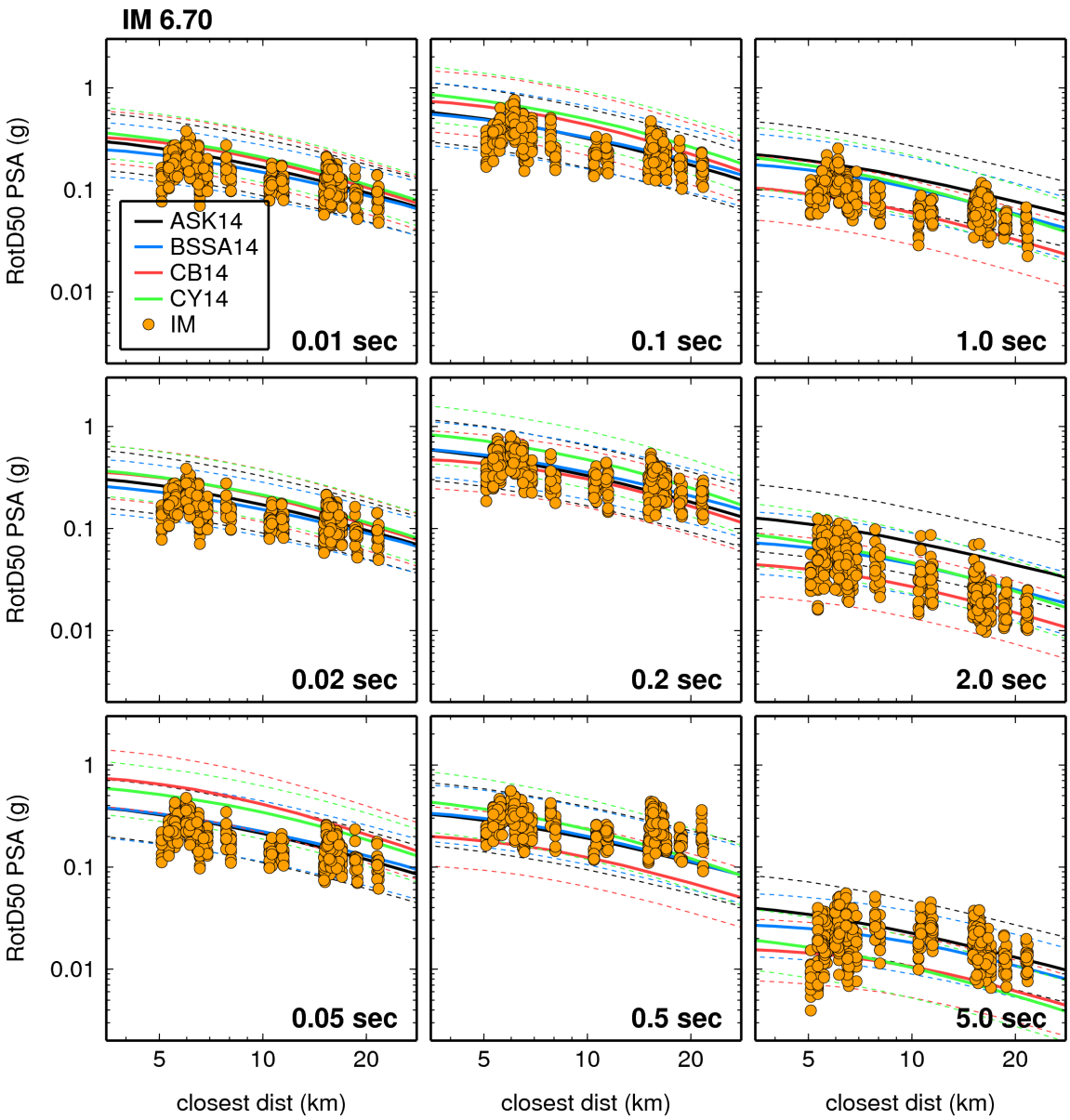

Figure 5b. Same as Figure 5a except simulated values are computed using the IM rupture generator.

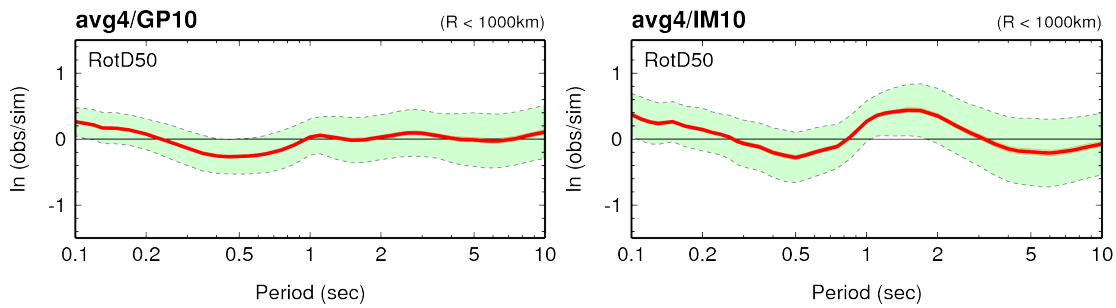

Figure 6. RotD50 horizontal spectral acceleration goodness of fit for the M6.7 scenario earthquake simulations averaged across ten realizations generated with GP (left panel) and IM (right panel) ruptures. The residuals used to determine the goodness of fit are computed between the simulations and the average of the median values from the four NGA-West2 GMPEs.

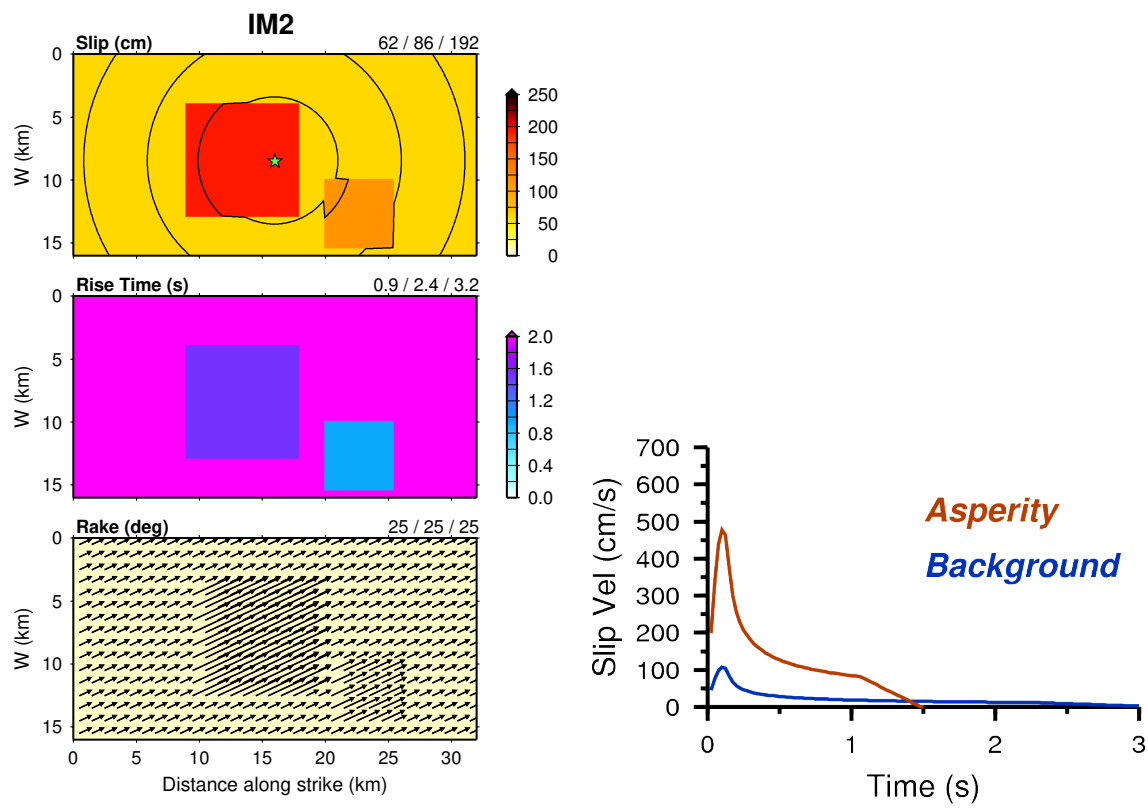

Figure 7. Example rupture generated with a modified version of IM (IM-fastRS) where the rupture speed is increased by 20% within the asperities (left panels). Slip velocity functions for the modified IM rupture taken from the largest slip asperity and background locations (right panel).

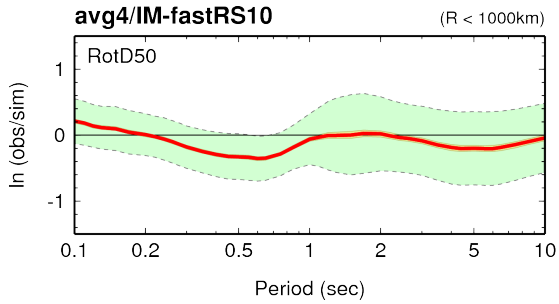

Figure 8. Same as Figure 6 except simulations use ruptures generated with IM-fastRS approach.

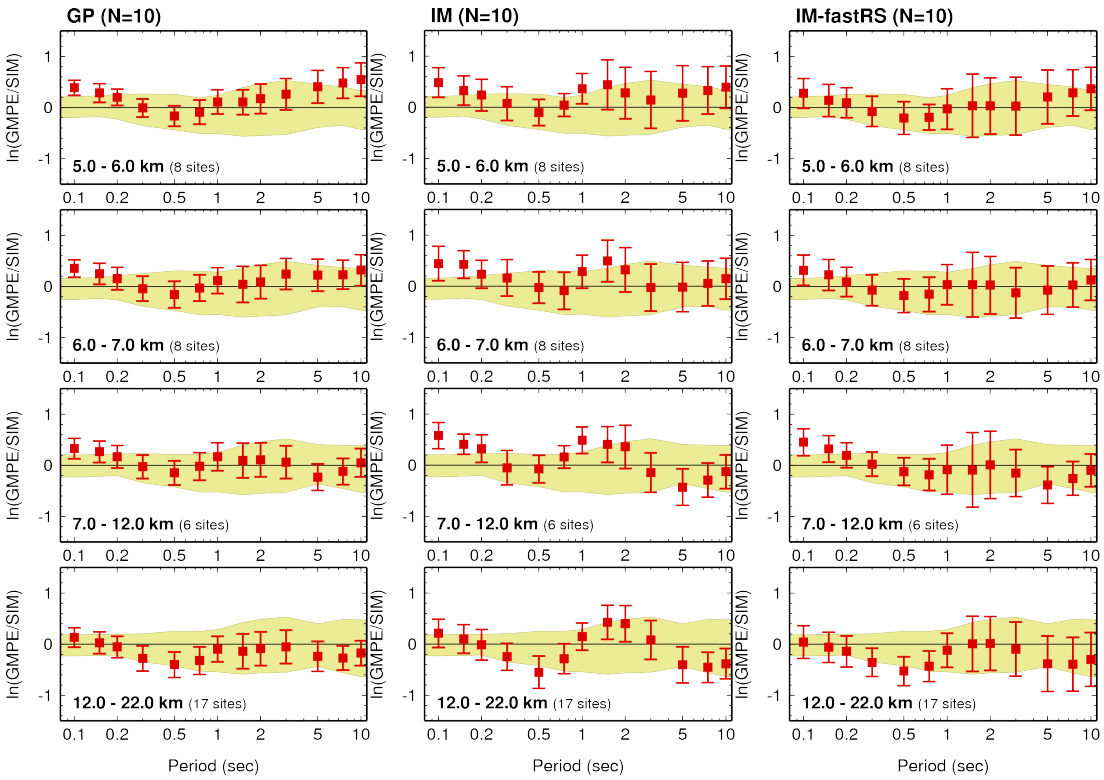

Figure 9. Residuals computed between median GMPE and simulated RotD50 ground motions and plotted as a function of the oscillator period for different distance bins. Results are shown for ruptures generated with GP (left panel), IM (middle) and IM-fastRS (right). Median GMPE values are determined across the four NGA-West2 relations for each period and station distance. The light-shaded region in each panel denotes the maximum and minimum deviation of the individual GMPE medians across the range of periods. At each

period, the median residual across the 10 simulated realizations is denoted by the square symbol with the error bars indicating the one standard deviation level of the residuals.

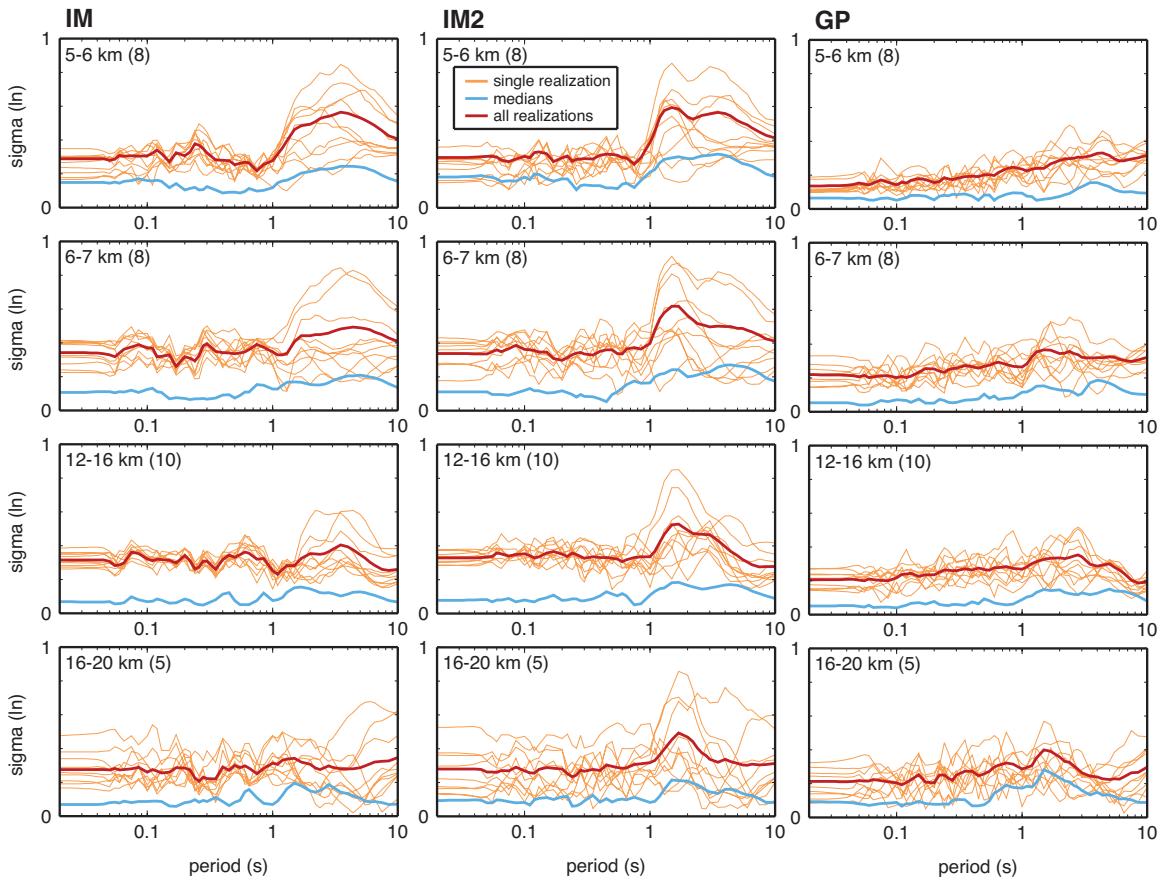

Figure 10. Standard deviation of simulated ground motion (orange traces), average standard deviation (red traces) and standard deviation of the median of simulated ground motion (blue traces) for IM, IM-fastRS and GP rupture generators. Each panel represents statistics obtained for the different distance bins indicated in each panel. The number of stations included in each distance bin is shown in parentheses.

Table 1. Fault Rupture Parameters

Magnitude	6.7
Strike	0°
Dip Angle	75°
Rake Angle	25°
Fault Length	32 km
Fault Width	16 km

Depth to the Top	3 km
Subfaults size	100m x 100m

Table 2. 1D Velocity Model

Depth (km)	V_p (km/s)	V_s (km/s)	Density (g/cm^3)	Q_p	Q_s
2.5	4.5	2.6	2.4	300	200
20.0	6.0	3.5	2.7	500	300
30.0	6.7	3.9	2.8	2000	1000
Half space	7.7	4.4	3.2	2000	1000

Table 3. Distance Bins

Distance Bin (km)	Number of Stations
5 – 6	8
6 – 7	8
7 - 12	6
12 – 22	17

Task 2. Strong Ground Motion Simulation Using a Characterized Source Model of the 2016 Kumamoto Earthquake

Introduction

The objective of this study is the simulation of strong ground motion from the 2016 Kumamoto earthquake, using the method of Graves and Pitarka (2015) (GP) and a characterized kinematic rupture model generated with the Irikura recipe (Irikura nd Miyake, 2011). GP is a hybrid method that contains three major parts. The first part is the kinematic rupture generator, the second is the ground motion simulator, and the third part performs empirical corrections for local site effects. Figure 1 shows the flowchart of the GP method. GP has been validated against recorded ground motion from several Californian earthquakes (Goulet et al., 2015). The method has not been fully tested against Japanese earthquakes, yet. GP uses a deterministic approach in computing the low frequency part of ground motion (<1Hz) and a stochastic approach (Boore 1983)in modeling the high frequency part of ground motion (>1Hz). For simulations performed in this study we substituted the GP rupture generator with the rupture generator of Irikura and Miyake (2011) (IM). IM follows a well-established scheme, calibrated with Japanese earthquake data. In a recent study Pitarka et al (2017) demonstrated that both GP and IM rupture generators perform equally well in the framework of the GP simulation method for moderate magnitude (M6.7) earthquakes. This study is a first attempt at applying the combination of GP method with the IM rupture model to simulating ground motion from a Japanese earthquake.

Characterized Rupture Model of the 2016 Kumamoto Earthquake

We used the Irikura recipe to produce a characterized rupture model for the M7.0 2016 Kumamoto earthquake. The fault length is 44 km and width is 18 km which yield a surface rupture of 792 km^2. The fault dimensions, as well as fault geometry were based on the fault rupture model proposed by Yoshida et al.,(2017). Their model was derived from the linear inversion of strong ground motion waveforms, performed in the frequency range 0.1-1Hz, using site specific 1D Green's functions. The fault model includes four segments that dip to the north-west of he fault trace. The faulting mechanism is predominantly of strike slip type. Figure 2 shows the location of the fault segments and seismic stations used in this study.

The main rupture parameters derived from the Irikura recipe are shown in Table 1. Based on the fault area scaling the recipe suggests two asperities with different kinematic characteristics and size. The average stress drop is 3.81 MPa, and average slip is 2.77 m. Since the objective here is to test the performance of the simulation scheme as well as that of the characterized rupture model at reproducing the recorded motion on a broad frequency range, the location of the asperities was chosen to be similar to that of the strong motion generation areas (SMGAs) proposed by Somei et al., 2017. Their SMGAs based model explains very well the overall broad-band characteristics of the recorded near-fault ground motion. In our model the small asperity was placed in the first fault segment while the second asperity extends to both second and third fault segments. The kinematic rupture

parameterization was performed following a two-step procedure. At first, the kinematic rupture model was generated for a planar fault geometry, and in a second step it was adopted to the target segmented fault geometry. No time delays were introduced when the rupture jumps between the fault segments. Following results from previous studies of the Kumamoto earthquake (e.g., Yoshida et al., 2016) the rupture velocity was set to a constant value of 2.8 km/s. In contrast to the SMGA's based rupture model, the asperities rupture initiation times and locations used in our model were not preassigned. Figure 3 shows the characterized rupture model used in our simulations.

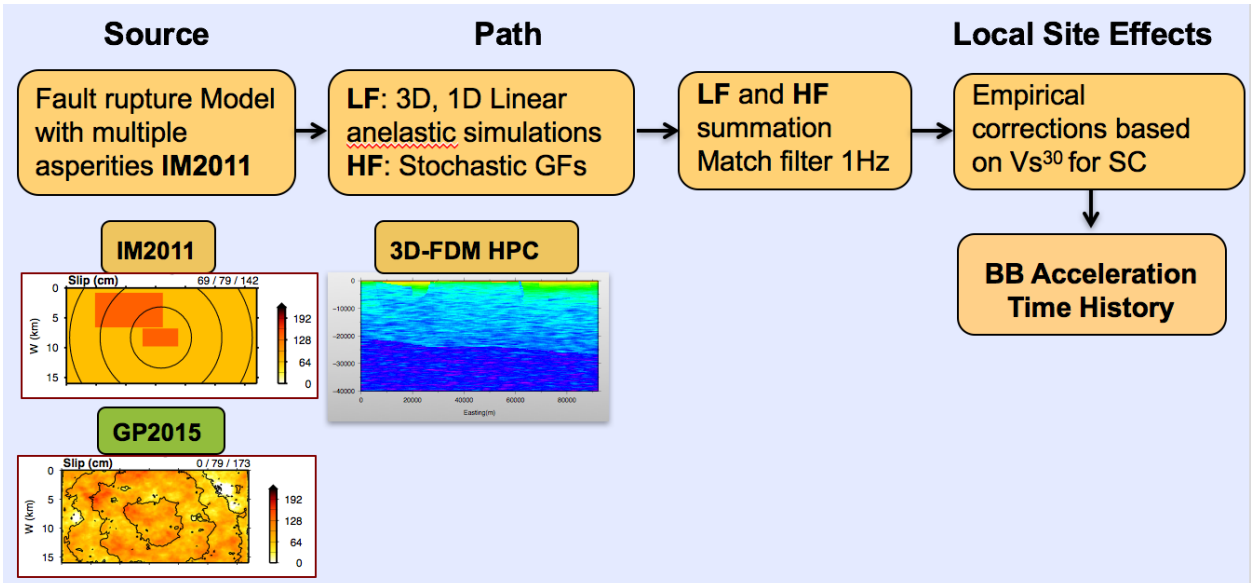

Figure 1. Flowchart of the Graves and Pitarka (2015) ground motion simulation method.

The underlying assumption of the characterized rupture model of Irikura and Miyake (2011) is that low frequency and high frequency parts of ground motion are generated mainly from the same rupture areas that are modeled as rupture asperities. This means that the slip and slip velocity are considered to be strongly spatially correlated. Observations show that while being strong for small and moderate earthquake, the correlation is weaker for M7 and larger earthquakes. Doe to the change in geophysical and rheological properties of the crustal material with depth, the shallow materials are less brittle. They can be characterized by weaker strength and weaker frictional properties than the deeper ones. Consequently, for large crustal earthquakes, which usually break the surface, the fracture energy consumed during the rupture propagation through shallow layers is relatively high. Therefore, the seismic energy generated by the shallow part of the fault is reduced. Moreover, the weakening of the surface material decreases the rupture speed and increases the rise time of the slip velocity. In addition, the reduction of peak slip velocity causes the amplitude reduction of the high frequency part of ground motion, typically observed during large earthquakes at short fault distances.. This phenomenon is well reproduced by spontaneous rupture modeling and multicycle simulations of long earthquake sequences (e.g., Pitarka et al., 2009 ; Dalguer et al.,2004).

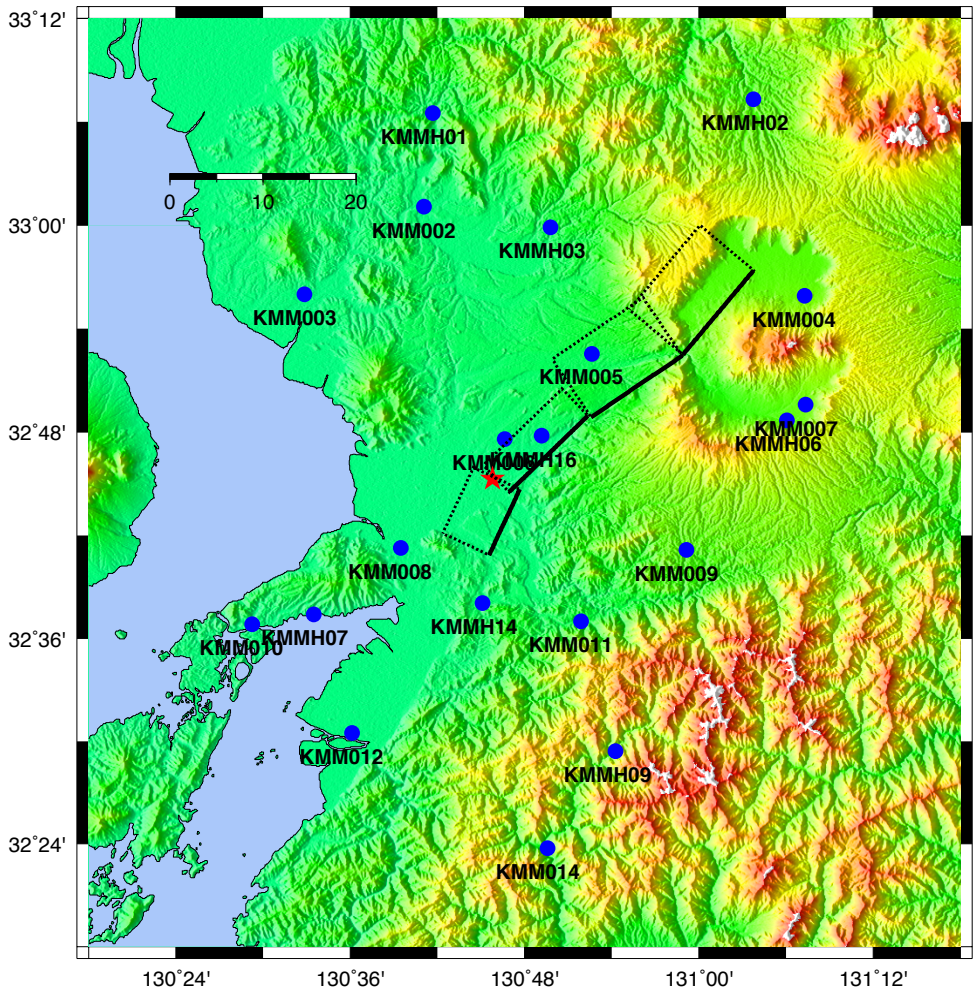

Figure 2. Map showing the fault trace (black lines), fault segments (dotted rectangles) and strong motion stations (blue circles). Red star indicates the epicenter location.

Strong Ground Motion Simulation Results

In computing the low frequency part of ground motion we used site specific 1D Green's functions calculated with 1D velocity models proposed by Yoshida et al (2016), and the frequency wave number method of Zhu and Rivera (2002). The fault area was divided into 200mx200m subfaults, and the subfault response was computed using a double-couple point source located at the center of the subfault. This refined source representation allows for accurate modeling of local rupture directivity.

The overall goodness of fit between the recorded and computed RotD50 (Boore, 2010) acceleration response spectra is shown in Figure 4. The model bias, computed as the log of the ratio between recorded and simulated acceleration response, as a function of period and averaged over 19 stations, is rather small at all periods. This result suggests that on average the simulation reproduces the overall characteristics of the recorded motion. In the GP

method, the amplitude of the simulated high frequency ground motion is mainly controlled by the stress drop parameter. For the simulation shown here the stress drop parameter was adjusted to 6.5MPa. For comparison, the stress drop parameter used in simulations of earthquakes in California is 5MPa, and for earthquakes in Central and Eastern US is 100-200 MPa. In terms of stress drop, our simulation suggests that the Kumamoto earthquake is similar to strike-slip earthquakes in California.

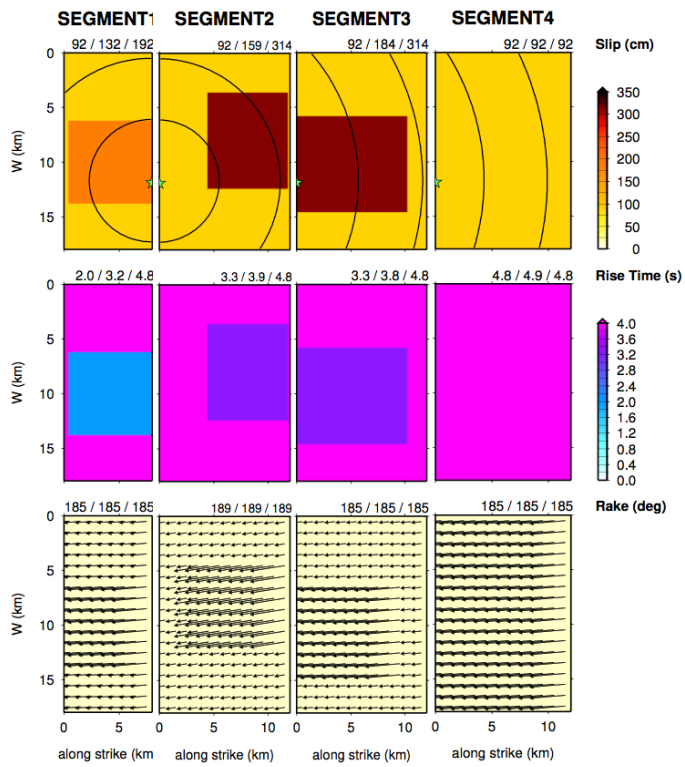

Figure 3. Characterized rupture of the 2016 Kumamoto earthquake obtained with Irikura and Miyake (2011) method: slip distribution (top panel), rise time (middle panel), rake vectors (bottom panel)

The comparison of the RotD50 acceleration response spectra at individual stations is shown in Figure 5. We concluded that the simulation performs better at near-fault sites, in particular, at sites located to the north west of the fault. The worse fit is obtained at station KMM004 where the 1D approximation of wave propagation underestimates the 3D wave propagation effects due to complex underground structure at the Aso volcano caldera. Similar misfit is obtained at KMM002, for periods longer than 1s. Our interpretation of these results is that the deficiency in long period energy of simulated ground motion is caused by combined weak directivity effect in the fourth segment of our fault model, and misrepresentation of potential strong 3D wave propagation effects by the 1D Green functions computed for this site.

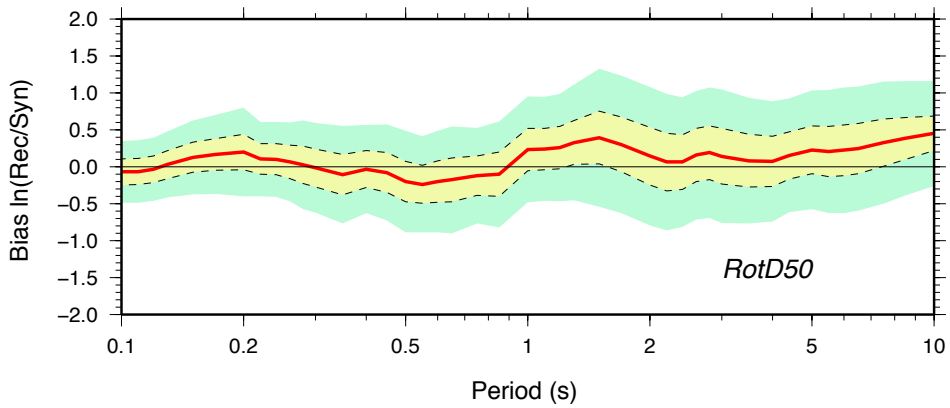

Figure 4. Goodness of fit for RotD50 horizontal response spectra using 19 stations. Red line shows the bias and dotted line shows the standard deviation of the bias.

The comparison of the acceleration and velocity time histories at all sites is shown in Figure 6 and Figure 7. The characterized model proposed here was simply based on the Irikura recipe. No attempts were made to improve the waveform fit by performing a complete study of the goodness of fit and its relation with the input parameter space. We recognize that in order to get the best waveform fit, the model should also contain details of rupture kinematics, including accurate asperities location and slip velocity distribution. From this point of view the waveform fit, and that of response spectra, obtained here, is satisfactorily.

The individual contributions of the rupture segments to simulated ground motion at selected stations is shown in Figure 8. In this figure we show acceleration time histories, computed at station KMMH16, located in the Mashiki town, and station KMM005 located further to the east. The waveform fit is very good at KMM005. In contrast, the waveform fit at KMH16 is rather poor, even though the fit of the response spectrum, which is affected by the overall characteristics of the ground motion, is very good. The ground motion recorded at these near-fault stations is largely affected by the source process. The simulation of the asperities contribution shows that both asperities have a significant effect suggesting that the recorded ground motion at the near-fault sites is a product of both forward and backward local rupture directivity effects.

Conclusions

The ground motion simulation of the 2016 Kumamoto earthquake at 19 strong motion sites, using the GP simulation method and a characterized rupture model produced with Irikura recipe, performed satisfactorily. The bias between the recorded and simulated Rod50 response spectra is small in the considered frequency range 0.1-10Hz. Our preliminary analysis of ground motion sensitivity to rupture model indicate that the characterized model is very robust. Analysis of the effects of the asperities location and rupture velocity are expected to improve the overall waveform fit especially at station KMMH16 which, as shown

here, is very sensitive to details of the local rupture kinematics. The analysis will be part of a future study aiming at understanding the separation of areas of large slip from areas of large peak slip velocity, and their effect on simulated ground motion.

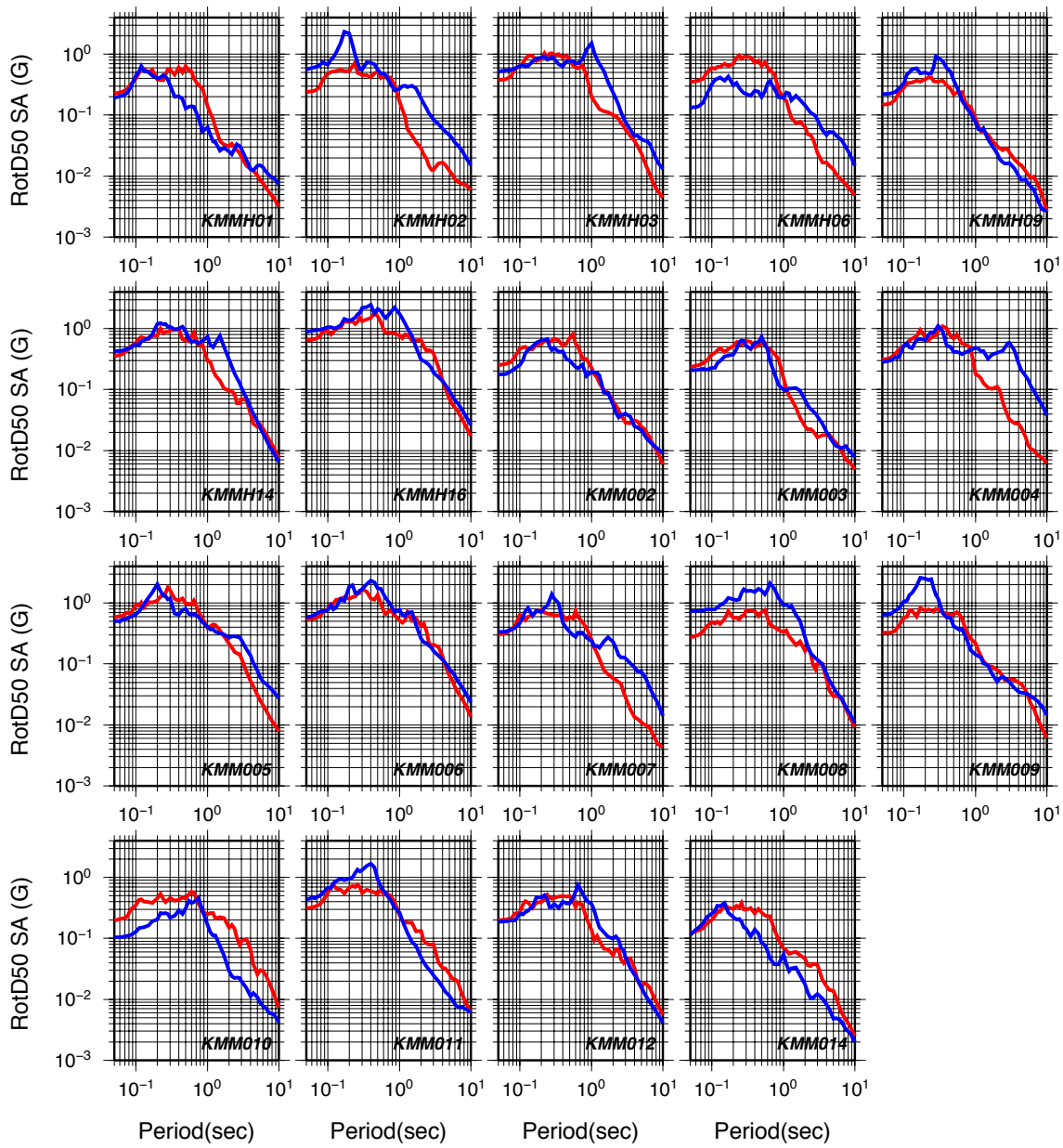

Figure 5. Comparison of recorded (red traces) and simulated (blue traces) RotD50 horizontal acceleration response spectra.

References

Boore D. (1983), Stochastic simulation of high frequency ground motions based on

seismological models of the radiated spectra. Bull. Seism. Soc. Am. 1983; 73: 1865-1894.

Boore, D. M., (2010). Orientation independent, nongeometric-mean measures of seismic intensity from two horizontal components of motion, Bull. Seism. Soc. Am. 100, 1830-1835.

Dalguer, L. A., H. Miyake, and K. Irikura (2004), Characterization of dynamic asperity source models for simulating strong ground motions, Proceedings of the 13th World Conference on Earthquake Engineering No. 3286.

Goulet, C. A., N. A. Abrahamson, P. G. Somerville, and K. E. Woodell (2015). The SCEC Broadband Platform validation exercise for pseudo-spectral acceleration: Methodology for code validation in the context of seismic hazard analyses, Seismol. Res. Lett 86, no. 1, doi: 10.1785/0220140101.

Graves, R., and Pitarka, A. (2015) Refinements to the Graves and Pitarka (2010) Broadband Ground-Motion Simulation Method Seismological Research Letters, January/February 2015, v. 86, p. 75-80, First published on December 17, 2014, doi:10.1785/0220140101

Irikura, K., and H. Miyake (2011). Recipe for Predicting Strong Ground Motion from Crustal Earthquake Scenarios, Pure Appl. Geophys. 168 (2011), 85–104 . DOI 10.1007/s00024-010-0150-9 .

Pitarka, A., L. A. Dalguer, S. M. Day, P. G. Somerville, and K. Dan (2009), Numerical Study of Ground-Motion Differences between Buried-Rupturing and Surface-Rupturing Earthquakes, Bull. Seismol. Soc. Am., 99(3), 1521–1537, doi:10.1785/0120080193.

Pitarka, A., R. Graves, K. Irikura, H. Miyake, and A. Rodgers (2017). Performance of Irikura Recipe Rupture Model Generator in Earthquake Ground Motion Simulations with Graves and Pitarka Hybrid Approach. Pure and Applied Geophysics (accepted for publication)

Zhu, L., and L. Rivera (2002). A note on the dynamic and static displacements from a point source in multilayered media, Geophys. J. Int. (2002) 148 (3): 619-627. doi: 10.1046/j.1365-246X.2002.01610.x

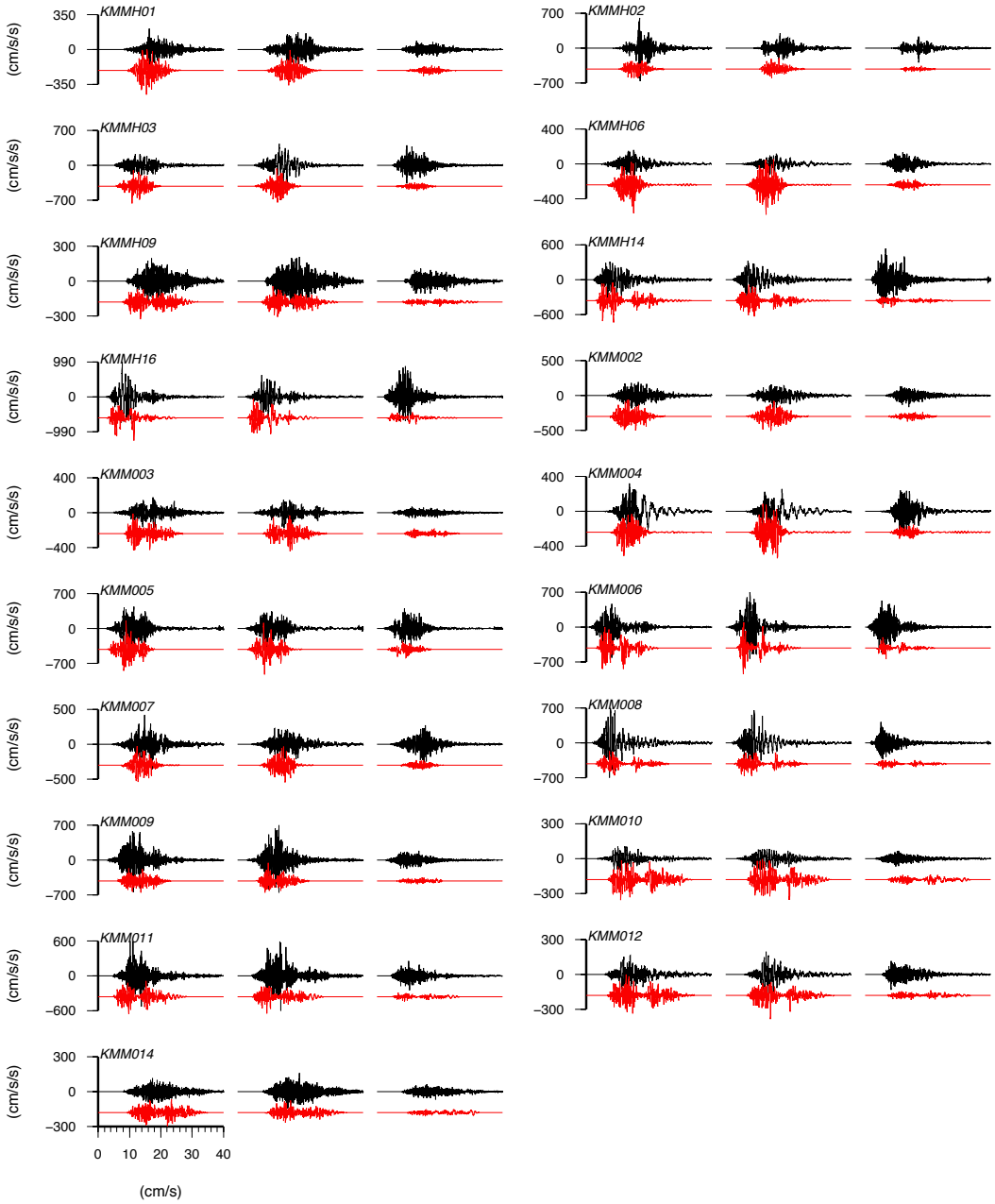

Figure 6. Comparison of recorded (black traces) and simulated (red traces) ground motion acceleration band-pass filtered at 0.02 -1.0.

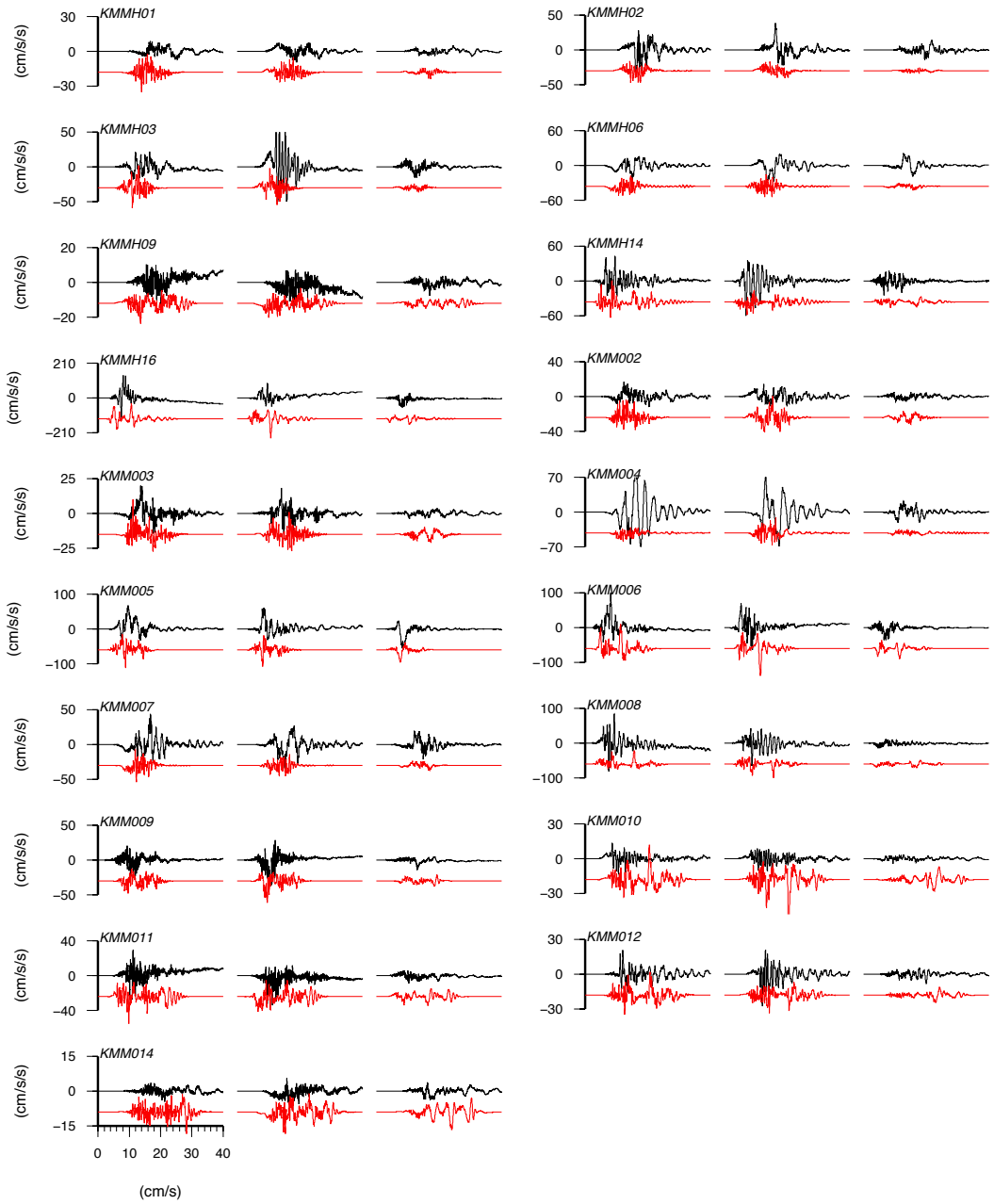

Figure 7. Comparison of recorded (black traces) and simulated (red traces) ground motion velocity band-pass filtered at 0.02 -1.0.

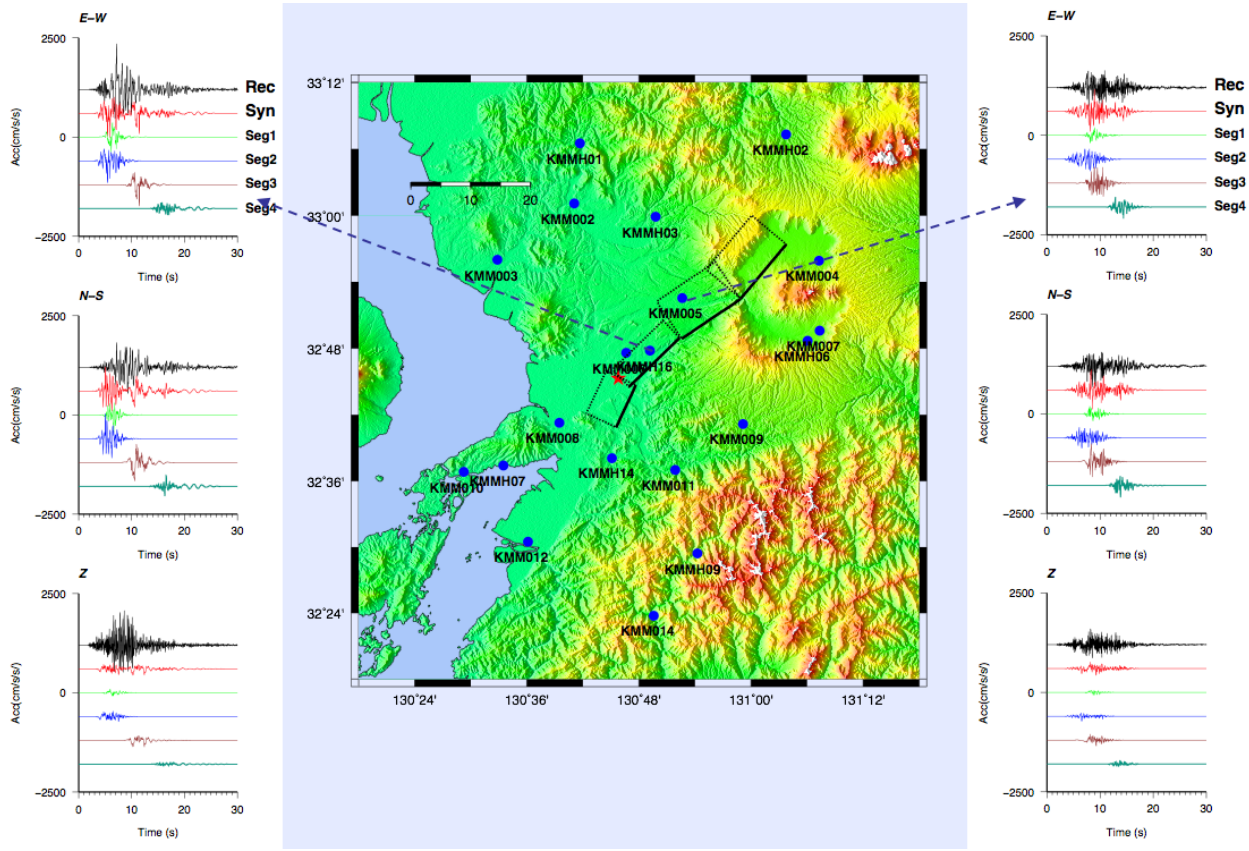

Figure 8. Contributions of individual fault segments to simulated ground motion at near-fault stations KMMH16, and KMM005. Black traces show the recorded acceleration, and the red traces show the simulated acceleration. The other traces show the individual contributions.

Table 1. Parameters of the characterized rupture model

Asperity 1 (segment 1)	*Asperity 2 (segment 2)*	*Asperity 2 (segment 3)*	*Background Area*
Length : 7.5 km Width : 7.4 km Vr : 2.8 km/s Slip : 192.2 cm Stress drop : 14.78 MPa	Length : 7.2 km Width : 8.6 km Vr : 2.8 km/s Slip : 313.8 cm Stress drop : 14.78 MPa	Length : 10 km Width : 8.6 km Vr: 2.8 km/s Slip : 313.8 cm Stress drop : 14.78 MPa	Slip : 0.9 m Stress drop : 2.92 MPa